Zinc Remediation by Zero-Valent Iron and the Associated Isotope Fractionation: Batch Experiments

by

Lingyi Kong

A thesis
presented to the University of Waterloo
in fulfillment of the
thesis requirement for the degree of
Master of Science
in
Earth Sciences

Waterloo, Ontario, Canada, 2017

Authors' Declaration

This thesis consists of material all of which I authored or co-authored: see Statement of Contributions included in the thesis. This is a true copy of the thesis, including any required final revisions, as accepted by my examiners.

I understand that my thesis may be made electronically available to the public.

Statement of Contribution

I completed the majority of the contributions, including experimental set up, sample collection, sample analysis, data analysis, figure preparations, and writing. Dr. Zou Finfrock and Dr. Ning Chen helped me to collect XANES (X-ray absorption near edge structure) and EXAFS (extended X-ray absorption fine structure) data. Dr. Ning Chen also contributed to the EXAFS data processing, modeling, and conceptual structure model preparation, and he also helped me to understand the EXAFS modeling. Joy SJ Hu contributed to analysis of the concentration of cations on ICP-OES (Inductively coupled plasma-optimal emission spectrometry). Dr. Jane Eagling contributed by teaching and giving advice on the improved purification method of Zn isotope analysis, and she contributed with edits and comments to improve this thesis. Emily Saurette helped me with the grammar correction and scientific writing in this thesis.

Abstract

Zinc is a bio-essential micro nutrient which is essential to the health of humans and other organisms. However, high Zn concentrations, as has been observed in mining waste water and urban runoff, can be harmful. The major remediation methods used to reduce the mobility of Zn in groundwater flow systems include Zn precipitation and adsorption. Zero-valent Iron (ZVI) has been used as a remediation material in permeable reactive barriers (PRBs), and it can be used to reduce the concentration of Zn in waste water. Measurements of Zn isotope ratios, may provide information to trace Zn(II) migration and help define reaction mechanisms during remediation of Zn contamination using ZVI. Laboratory batch experiments, combined with traditional geochemical analysis, non-traditional stable isotope analysis and solid-phase analysis (XANES and EXAFS) were used to evaluate Zn removal mechanisms associated with ZVI in differing initial Zn-bearing solutions and with varying alkalinity concentrations. Decreasing concentrations of Zn were observed throughout all of the experiments. X-ray absorption near edge structure (XANES) and extended X-ray absorption fine structure (EXAFS) analyses indicted the presence of Zn(II) on the solid phase with a coordination number of four, compared to a coordination number of six in the initial solutions. Models based on the measurements of EXAFS were used to assess the possible products on the solid phases. The results suggest that a combination of sorption and precipitation mechanisms dominated the removal of Zn for all of the aqueous solutions. The decline in dissolved Zn concentrations was accompanied by a decreasing value of δ^{66}Zn in the experimental solutions, indicating preferential accumulation of ^{66}Zn in the solid phase. The differences in dissolved Zn solutions and alkalinity did not significantly affect the extent of Zn isotope fractionation. The change in Zn concentration and δ^{66}Zn can be fit with equilibrium fractionation models. The fractionation factors were similar for all batch experiments,

reflecting the consistent change in coordination. The fractionation factors, which were calculated from the fitting process, cannot separate sorption-dominated and precipitation-dominated removal mechanism in these experiments.

Acknowledgements

I would like to give my appreciation to my supervisor, Dr. David Blowes, for inspiring me to find my interest in geochemistry, especially in non-traditional stable isotopes. Without him, I would not have had the great opportunity to work on this interesting project and work on isotopes in a clean lab. He offered me guidance and support with my academic research, critical thinking and scientific writing. He encouraged me to work and think independently, and patiently gave me advice. He taught me to be creative and precise during my research.

I would like to thank my committee members, Dr. Carol Ptacek and Dr. Richard Amos, for providing me with valuable comments on my research and writing. Their passion for research and constant encouragement are a motivation for me to complete this research.

My grateful acknowledgements are extended to Dr. Ning Chen and Dr. Zou Finfrock, for their assistance with my EXAFS results. Without their solid knowledge and depth of experience, this work would not be possible.

I appreciate my colleagues in the GGR group. Dr. Jane Eagling supported me a lot during my research, and she always encouraged me when I encountered challenges. She is not only my mentor for my research, she is also a great friend. Thank you to Julia Jamieson-Hanes, Heather Shrimpton and Roberta Parigi, who shared their experiences with non-traditional stable isotopes to me without reservation. They always answered my questions with patience. Thank you to Joy S.J. Hu for helping me to analyze my samples on ICP-OES, and thank you to Laura Groza for technical support. Thank you to Filip Budimir, Justin Buis and Jeff Leon. I am so glad we can work on the same project and work out the problems we face together. My appreciation also goes out to my friends Alana Wang, Colleen Atherton and Emily Saurette, for the happy times we had together.

I want to thank all my friends who accompanied me during my graduate studies. In particular, thanks to Luqi Cui, Hexin Wang, Ying Wang, Yuyi Jin, Kai Liu and Xinze Lu. They make me into the person I want to be.

Finally, I heartily thank my parents and my boyfriend Jiangyue Ju, who always support me whenever I need them. Without them and their love, I could not finish this work. They always encourage me to pursue my interests and dreams, and they gave me the courage to be successful.

Table of Contents

List of Figures

List of Tables

Chapter 1: Introduction

Zinc is a bio-essential trace nutrient for nearly all organisms, and can become toxic at high concentrations (Allen et al., 1983). Both sorption and precipitation limit the mobility of Zn in groundwater (Roberts et al., 2003; Ha et al., 2007). Passive remediation technologies, such as treatment using zero-valent iron (ZVI), have been used at sites contaminated with heavy metals due to the relatively low cost of ZVI and suitable reaction rates (Blowes et al., 1999; Jamieson-Hanes et al., 2014). The processes that control Zn mobility, including precipitation, dissolution and sorption, result in Zn isotope fractionation. Because Zn undergoes limited fractionation, extended X-ray absorption fine structure (EXAFS) was used with traditional aqueous geochemical analyses and measurements of Zn isotope ratios to understand the mechanisms controlling the attenuation of Zn under anaerobic static saturated- conditions. In addition, another goal of this research is to assess whether differences in Zn aqueous solutions ($ZnSO_4$ and $ZnCl_2$) or differences in alkalinity, impact isotope fractionation and the remediation mechanisms. This chapter provides background information regarding the behavior of Zn in groundwater, a brief overview of the ZVI/H_2O system, a review of Zn isotope fractionation and the relationship between Zn coordination number changes and isotope fractionation.

1.1 Background

1.1.1 Zn in the environment

Zinc is a bio-essential micronutrient for most organisms, and it is ubiquitous in soils, sediments, water system and the biosphere. It is an essential cofactor of more than 300 enzymes and required for cell growth (Plum et al., 2010). Both Zn deficiency and excess have a negative

impacts on human health, for example, excess levels of Zn may alter lymphocyte function and cause copper deficiency (Plum et al., 2010).

Zinc can be released into the environment by natural processes, such as during the weathering of Zn-bearing minerals including spalerite (ZnS) and smithsonite ($ZnCO_3$). Elevated aqueous concentrations of Zn in soil and water systems are also associated with anthropogenic activities, such as atmospheric emissions from metallurgical industries, slurry spreading of swine manure, urban road runoff, mining wastes and smelter slags (Juillot et al., 2011; Matthies et al., 2014). De Giudici et al. (2008) and Medas et al. (2012) reported the Zn concentration exceeded 100 mg L^{-1} in the mine drainage in the stream in southwestern Sardinia, Italy, the Rio Naracauli. At the former Sherritt-Gordon Mine, located in Sherridon Manitoba Zn concentrations of up 55000 mg L^{-1} were observed in the pore water of a tailings impoundment, and up to 155 mg L^{-1} Zn were observed in the impoundment effluent (Moncur et al., 2005; Moncur et al., 2012) In Canada, the regulatory drinking water limit for Zn is 5 mg L^{-1} (Health Canada, 2017), and for the protection of freshwater aquatic life Zn concentrations cannot exceed 34 μg L^{-1} (Canadian Council of the Ministers of the Environment [CCME], 2016).

Under normal environmental conditions, Zn predominately exists in the 2+ oxidation state, and its fate is dominantly controlled by sorption and precipitation. Zinc mobility is limited by precipitation of zinc hydroxide ($ZnOH_2$) in systems with pH greater than 8, and smithsonite ($ZnCO_3$) or hydrous Zn carbonate minerals when the pH increases from 7.5 to 8.2 (Nuttall and Younger (2000). Compared to the precipitation rate of smithsonite, zinc hydroxide precipitates faster (Patterson et al., 1977). When dissolved sulfide is in contact with Zn, zinc sulfide will form and limit the mobility of Zn.

Zinc sorbs to soil comprised predominately of inorganic clays (Viers et al., 2007), iron and

manganese oxides and hydroxides (Balistrieri et al., 2008; Bryan et al., 2015; Lemarchand et al., 2007; Pokrovsky et al., 2005; Swedlund et al., 2009), metal carbonates and phosphates (Bradl, 2004). Thus Zn can be released to the aqueous phase by reductive dissolution of iron and manganese oxides and hydroxides under oxygen deficient conditions. Under aerobic conditions, Zn can partition onto iron oxyhydroxides, iron and manganese oxides (Balistrieri et al., 2008; Bryan et al., 2015; Lemarchand et al., 2007; Pokrovsky et al., 2006; Pokrovsky et al., 2005; Reynolds, 2012; Swedlund et al., 2009), granular zero-valent iron (Lindsay et al., 2008; Wilkin & McNeil, 2003), clay minerals (Lin & Juang, 2002; Sheta et al., 2003) and organic materials. The relative sorption efficiency of these materials is a function of pH, oxidation/ reduction potential (Eh), salinity, concentrations and nature of complexing ligands, cation exchange capacity, and the concentration of Zn.

1.1.2 Treatment of Zn by Zero-valent Iron

Zero-valent Iron (ZVI) has been used as a treatment media to mitigate highly mobile contaminants in groundwater for more than two decades (Blowes et al., 1996; Blowes et al., 1999; Cantrell et al., 1995; Katsoyiannis et al., 2015; Lindsay et al., 2008). Zero-valent Iron has been successfully used for permeable reactive barriers (PRBs) and for the reduction of source contamination (Blowes et al. 1999). The corrosion of ZVI under anaerobic conditions was reported by Agrawal & Tratnyek (1996) as,

(1) $$2H_2O + Fe^0\,(s) \rightarrow Fe^{2+} + 2OH^- + H_2\,(aq)$$

During this iron corrosion process, the metallic iron is oxidized to ferrous iron leading to an increased pH, a decreased oxidation-reduction potential (ORP) and yielding $H_{2(g)}$. Ferrous iron ions (Fe^{2+}) are not stable in the presence of species which have higher oxidation states (e.g.

Cr(VI), As(V) and Se(VI)). Subsequently, ferric iron (Fe^{3+}) is formed by the oxidation of ferrous iron (Fe^{2+}), and the oxidized Fe^{3+}, which hydrolyses and precipitates as ferric (oxy)hydroxide phases.

In the Fe^0-H_2O system, the possible contamination removal mechanisms include: 1) reduction and precipitation of contaminants to lower oxidation states (Jamieson-Hanes et al., 2014); 2) mineral precipitation caused by increased pH; and 3) adsorption to or co-precipitation with newly formed poorly crystallized iron hydroxides and oxides (Klimkova et al., 2011; Li and Zhang, 2007; Wilkin and McNeil, 2003). These removal mechanisms can occur simultaneously and contaminant removal may be due to more than one mechanism.

As the standard potential E^0 of Zn (-0.76 volts) is slightly lower than Fe (-0.41 volts) (Li and Zhang, 2007) Zn can be considered to have one oxidation state (Zn^{2+}) in the ZVI treatment systems in this study. Therefore, the most important removal mechanisms are sorption and surface complex formation or Zn precipitation, or a combination of these processes.

1.1.3 Zn isotope measurements

Zinc has five stable isotopes ^{64}Zn, ^{66}Zn, ^{67}Zn, ^{68}Zn and ^{70}Zn, with average natural abundances of 48.63, 27.90, 4.10, 18.75, and 0.62%, respectively (Rosman and Taylor, 1998). Multicollector inductively coupled plasma mass spectrometry (MC-ICP-MS) can be used to measure variations in the composition of Zn isotopes (Cloquet et al., 2008) and attain a precision level that is lower than 0.05‰ per mass unit (Maréchal et al., 1999). With the help of purification methods, for example those introduced by Maréchal et al. (1999), and the double spike technique, greater precision can be achieved by reducing the isobaric interferences on Zn, adjusting for isotope fractionation during purification and instrumental mass bias.

Although there are other expression methods, Zn isotope ratios in this thesis are expressed as $^{66/64}$Zn because ^{64}Zn and ^{66}Zn have relatively high abundances, and $^{66/64}$Zn ratios have been used to report Zn isotope ratios in previous research. Delta notation in per mil is used to determine Zn isotope ratios as,

(2) $$\delta^{66}Zn = \left[\frac{(^{66}Zn/^{64}Zn)_{sample}}{(^{66}Zn/^{64}Zn)_{IRMM-3702}} - 1\right] \times 1000‰$$

The delta $\delta^{66}Zn$ values reported in this thesis are relative to the standard IRMM-3702. Another standard (JMC Lyon Zn) has been used to report Zn isotopes in previous papers. Based on the research of Moeller et al. (2012) the ratio of $^{66/64}Zn_{IRMM-3702}$ is -0.29±0.05‰ when JMC Lyon is used as a standard. Thus, the value of δ^{66}Zn reported to standard JMC can be converted to the one reported to standard IRMM-3702, following,

(3) $$\delta^{66}Zn_{IRMM-3702} = \frac{\delta^{66}Zn_{JMC}+0.29}{0.99971}$$

This conversion was made to compare to previous Zn isotope measurements determined using JMC Lyon standard instead of IRMM-3702 standard.

1.1.4 Zn isotope fractionation

Different isotopes of an element have similar chemical and physical properties. However, when different isotopes are involved in reactions the slight differences in mass between the isotopes can manifest into significant differences during physical, chemical and biological processes. In the mass-dependent reactions, the relative proportion of isotopes changes to a new and unique ratio. Thus, the isotope ratio is considered an indicator of the source of the isotopes produced in a reaction, or, the specific reaction mechanism. Zinc isotope fractionation has been

reported during sorption (Balistrieri et al., 2008; Bryan et al., 2015; Juillot et al., 2008; Pokrovsky et al., 2005), precipitation (Veeramani et al., 2015), reduction (Kavner et al., 2008), chemical diffusion (Rodushkin et al. 2004), and biological incorporation (Kafantaris and Borrok, 2014).

Zinc isotope ratios have been reported as indicators in terrestrial minerals, marine sediments and biological materials. In addition, significantly different Zn isotope ratios were found in anthropogenic contamination in water samples, watersheds, wetlands, ore deposits, and waste-rock drainage (Matthies et al., 2014; Juillot et al., 2011; Borrok et al., 2008; Mason et al., 2005; Viers et al., 2007). The isotopic fractionation between terrestrial minerals and marine sediments can indicate the physical weathering and chemical separation of Zn isotopes. Fractionation is found during mineral precipitation along hydrothermal fluid pathways (Yamakawa et al. 2009). Laboratory experiments have demonstrated that fractionation can either be negative or positive during Zn adsorption onto oxides and hydroxides depending on mineral species and pH (Balistrieri et al., 2008; Juillot et al., 2008; Pokrovsky et al., 2005); Veeramani et al. (2015) reported a positive Zn fractionation in the dissolved Zn isotopic ratio associated with the precipitation of sphalerite (ZnS), and negative fractionation in conjunction with precipitation of hydrozincite ($Zn_5(CO_3)_2(OH)_6$) and hopeite ($Zn_3(PO_4)_2 \bullet 4H_2O$).

Zinc does not undergo redox reactions in standard surficial environmental conditions; thus isotope fractionation is considered to occur as a result of changes in Zn coordination number (Maréchal and Albarède, 2002). Zinc occurs as hexa-aqua ions or tetra-aqua ions with a coordination number of six or four (Bryan et al. 2015). The heavier isotope is preferentially concentrated in sites with stronger bonds and therefore smaller coordination number (Bigeleisen and Mayer, 1947; Schauble, 2004). The dominant Zn species present in aqueous solution is

$Zn(H_2O_6)^{2+}$, in which Zn forms an octahedral structure with a coordination number of six or seven (Balistrieri et al. 2008; Bryan et al. 2015; Cloquet et al. 2008). A tetrahedral oxygen Zn structure with coordination number of four in the solid phase was reported by Balistrieri et al. (2008), Bryan et al. (2015) and Juillot et al. (2008) and is associated with a negative Zn isotope fractionation in the aqueous phase.

1.2 Research Objective

The primary goal of this thesis is to characterize Zn isotope fractionation during treatment of dissolved Zn with ZVI, exploring the influence of starting material ($ZnSO_4$ vs. $ZnCl_2$) and increasing alkalinity. Characterizing Zn isotope fractionation associated with removal mechanisms will improve the ability to trace Zn mobility and identify reaction mechanisms in groundwater flow systems through the analysis of isotope ratios. This research combins traditional geochemical analysis, Zn isotope ratio measurements and solid-phase analysis to provide more information about the structure of Zn reaction products produced during remediation, the relationship between isotope fractionation and the local fine structure, the potential treatment mechanisms, reaction rates, and the reaction efficiency. The objectives of this research are to:

- Measure changes in Zn isotope ratios during treatment with ZVI under steady-state, anaerobic conditions;
- Assess the influence of different Zn salt solutions and aqueous matrices (i.e. alkalinity);
- Combine solid phase analysis and isotope ratio measurements to identify potential removal mechanisms of Zn;

- Evaluate the relationship between Zn isotope fractionation and the change in Zn local fine structure.

1.3 Thesis Organization

This thesis includes three chapters. Chapter 1 introduces the necessary background information for this research. Chapter 2 describes the experiments including the methods, results and discussion. Lastly, Chapter 3, provides a summary of the findings and recommendations for future work.

Chapter 2: Isotopic Fractionation During Removal of Zinc by Zero-valent Iron (ZVI)

2.1 Summary

Zinc has five isotopes (^{64}Zn, ^{66}Zn, ^{67}Zn, ^{68}Zn and ^{70}Zn) which can undergo fractionation during different reaction processes, and thereby can be used as a tool to understand Zn attenuation mechanisms during remediation. Zero Valent Iron (ZVI) is used widely for the treatment of heavy metal contamination especially in permeable reaction barriers (PRB). In this study, batch experiments were conducted to simulate the anaerobic conditions found in sub-surface environments that contain ZVI as a treatment material to (1) compare the effect of different input aqueous solutions and (2) understand the impact of increased alkalinity on the rate and extent of Zn attenuation and the associated isotope fractionation.

Environmentally relevant Zn solutions ($ZnCl_2$ and $ZnSO_4$) were chosen for this study to investigate how using different Zn salts might influence Zn attenuation, removal mechanisms, and the associated Zn isotope fractionation during treatment with ZVI. Zinc sulfate was chosen because sulfate is a common co-contaminant, especially at sulfide-bearing mine sites. Zinc chloride was chosen because of its high solubility, and because it has been used in previous Zn isotope studies (Juillot et al., 2008; Veeramani et al., 2015). The impact of increased alkalinity on the behavior of Zn was assessed by using ultra-pure water, and ultra-pure water amended with 10 mg L^{-1} $CaCO_3$ in a solution containing a Zn(II) concentration of 5 mg L^{-1}. The solid ZVI was examined by X-ray absorption near edge structure (XANES) and extended X-ray absorption fine structure (EXAFS) spectroscopy in order to examine the oxidation state, coordination environment and local structure of Zn associated with the ZVI. Results from this study demonstrate that precipitation and/or adsorption are the major mechanism that remove Zn from

solution and result in a change in $\delta^{66}Zn$ signature that was small and negative. In addition, the presence of different counter ions (Cl^- or SO_4^{2-}) or increased alkalinity did not significantly affect Zn isotope fractionation. These results suggest that the observations of Zn isotope fractionation can be applied to a broader range of scenarios, and extending the potential for utilization of Zn isotope ratio measurement.

2.2 Introduction

Zinc is a naturally abundant element in water, and it is a bio-essential trace nutrient for all living organisms (Plum et al., 2010). Anthropogenic impacts, including atmospheric metallurgic industrial emissions, swine-manure spreading, urban road run off, mining wastes and smelter slags, have led to elevated concentrations of Zn in the environment. For example, Zn concentrations ranging from less than 1 mg L^{-1} to 55000 mg L^{-1} have been reported in industrial discharges and acid mine drainage (Bigalke et al., 2010; Deliyanni et al., 2007; Fernandez and Borrok, 2009; Juillot et al., 2011; Maréchalet al., 1999; Moncur et al., 2005; Moncur et al., 2012). At elevated concentrations, Zn is harmful to sensitive biota, such as salmon (Weis and Weis, 1991) and vegetation (Eisler, 1993). Zinc exists in the 2+ oxidation state in the natural environment, and it is not considered redox sensitive under most natural conditions (Cloquet et al., 2008). Sphalerite (ZnS) and smithsonite ($ZnCO_3$) are the two most significant Zn ores in the geosphere (Cloquet et al., 2008).

Techniques such as coagulation-flocculation, membrane processes, ion exchange resin and activated carbon can be used to treat Zn wastewater in order to meet regulatory concentration limits, however these treatments are expensive, require ongoing maintenance and are inefficient at low metal concentrations (Deliyanni et al., 2007; Karabulut et al., 2000; Veeken et al., 2003).

Hence, precipitation, which has a relatively low cost (Veeken et al., 2003), and adsorption, which is effective at low metal concentrations (Karabulut et al., 2000), are becoming more popular treatment technologies. Hydroxide ($Zn(OH)_2$), sulfide (ZnS), hydrozincite ($Zn_5(CO_3)_2(OH)_6$), and smithsonite ($ZnCO_3$) precipitation were reported as effective methods to remove Zn from industrial and mine wastewaters (Brooks, 1986; Nuttall and Younger, 2000; Veeken et al., 2003). Sorbents such as iron and manganese oxide (Balistrieri et al., 2008; Bryan et al., 2015; Lemarchand et al., 2007; Pokrovsky et al., 2005; Pokrovsky et al., 2006; Reynolds, 2012; Swedlund et al., 2009), (Wilkin and McNeil, 2003) and clay minerals (Lin and Juang, 2002; Sheta et al., 2003) have been used to remove Zn from solutions.

Passive remediation technologies, including permeable reactive barriers containing reactive media such as zero-valent iron (ZVI), have been used to remediate contaminated groundwater for more than two decades (Blowes et al., 1999). Advantages of ZVI barriers include low cost, large treatment capacities and effective remediation of heavy metals when compared to other treatment methods. During the remediation process, ZVI can be used as a reductant that can reduce the heavy metals, or provide a substrate for sorption, co-precipitation or precipitation reactions.

Zinc has five stable isotopes ^{64}Zn, ^{66}Zn, ^{67}Zn, ^{68}Zn and ^{70}Zn, with average natural abundances of 48.63, 27.90, 4.10, 18.75, and 0.62% respectively (Rosman and Taylor, 1998). Zinc isotopes have been used as a tool to fingerprint Zn sources and elucidate the mechanisms controlling the transport, attenuation and cycling of Zn (Borrok et al., 2008; Gélabert et al., 2006; Juillot et al., 2011; Mason et al., 2005; Matthies et al., 2014; Veeramani et al., 2015; Viers et al., 2007; Weiss et al., 2005; Wilkinson et al., 2005).

Zinc exists in the 2+ oxidation under most environmentally relevant conditions and therefore changes in isotope fractionation are related to changes in the coordination environment. For

example, the coordination of Zn^{2+} in dilute aqueous solutions is usually octahedral; however, when Zn has a bond with oxygen or sulfur, it is commonly in tetrahedral coordination. In the shift to tetrahedral coordination preferential incorporation of heavier Zn isotopes is expected, because smaller coordination numbers are generally associated with stronger bonds and a preference for heavier isotopes (Bigeleisen and Mayer, 1947; Schauble, 2004). The isotope fractionation associated with adsorption is variable. Fractionation may be negative or positive depending on the minerals (adsorbate) present, aqueous species, pH, and ionic strength or concentration (Cloquet et al. 2008). The difference in the reported magnitudes of isotope fractionation may be attributed to the structural differences of the adsorbed Zn (Juillot et al., 2008).

Zinc precipitation can result in either negative or positive isotope fractionation. For example, through the precipitation of sphalerite (ZnS), the lighter Zn isotope (^{64}Zn) is preferentially removed from the aqueous phase leading to a negative fractionation factor (ε) -0.30 ‰. However, during the precipitation of hydrozincite ($Zn_5(CO_3)_2(OH)_6$) and hopeite ($Zn_3(PO_4)_2 \cdot 4H_2O$), the enrichment of the light Zn isotope in aqueous solution reservoirs leads to a positive fractionation factors (ε) 0.18, and 0.25 ‰ (Veeramani et al., 2015).

The chemical bonds formed during precipitation and adsorption of Zn impact the magnitude of Zn isotope fractionation in different degrees. Extended X-ray absorption fine structure (EXAFS) spectroscopy is utilized to analyze thestructure of the solid phase and help assist in the interpretation of isotope ratio measurements.

2.3 Experimental Methods

2.3.1 Batch Experiments

Batch experiments were conducted with different Zn salts and solution matrices to evaluate Zn removal and associated isotope fractionation during reaction with ZVI in anaerobic environments. The batch experiments included four independent experiments summarized in Table 1.

Table 1 Metal salts and solutions of four batch experiments

Experiment	Metal salt and solution
BT1	4.883 mg L^{-1} Zn^{2+} as $ZnSO_4$ in ultra-pure water
BT2	4.763 mg L^{-1} Zn^{2+} as $ZnCl_2$ in ultra-pure water
BT3	4.859 mg L^{-1} Zn^{2+} as $ZnSO_4$ in 10 mg L^{-1} $CaCO_3$ solution
BT4	4.497 mg L^{-1} Zn^{2+} as $ZnCl_2$ in 10 mg L^{-1} $CaCO_3$ solution

Different Zn solutions were chosen for this study to investigate whether different Zn species influence the removal mechanism. Zinc sulfate was chosen because SO_4^{2-} is a common co-contaminant reported at mine sites, especially in acid mine drainage; zinc chloride was chosen because of its high solubility, and it has been used in previous Zn isotope studies (Juillot et al., 2008, Veeramani et al., 2015). Ultra-pure water and 10 mg L^{-1} $CaCO_3$ were used as matrix solutions to evaluate the impact of increasing alkalinity. All four experiments were conducted in an anaerobic chamber (Coy Laboratory Products Inc., Grass Lake, MI) with a 3% H_2/balance N_2 atmosphere to simulate anoxic groundwater conditions.

Zero-valent iron was prepared for use in the batch experiments by sieving to obtain particles between 0.25 – 1.19 mm (16 to 60 mesh). Oxide coatings on the surface of the ZVI were removed by immersing it in 1.2 M HCl. After immersing for a few hours the solution was

decanted and replaced and this process continued until the ZVI changed in color from rust brown to black. After the last wash in 1.2 M HCl, ZVI was submerged in 0.12 M HCl and transferred into the anaerobic glovebox, where the ZVI was rinsed by vacuum filtration with Ar-purged ultra-pure Milli-Q® water to remove any acid residues.

Zinc sulfate (ZnSO4) and zinc chloride ($ZnCl_2$) stock solutions were prepared by dissolving reagent grade $ZnSO_4 \bullet 7H_2O$ and $ZnCl_2$ salts in ultra-pure water to achieve ≈ 500 mg L^{-1} Zn in solution. The concentration of Zn in the stock solutions was confirmed by ICP-OES. Calcium carbonate saturated water was prepared by adding calcium carbonate salts to ultra-pure water (0.1 g L^{-1} $CaCO_3$), and solution was bubbled with CO_2 to help $CaCO_3$ dissolve.

The Zn input solutions used in BT1 and BT2 were prepared by diluting the respective stock solutions (i.e. $ZnSO_4$ and $ZnCl_2$) with ultra-pure water whilst BT3 and BT4 were prepared using, 10 mg L^{-1} $CaCO_3$ to give a final concentration of 5 mg L^{-1} Zn. Input solutions were purged with Ar to remove O_2 and excess CO_2 and equilibrated in the anaerobic chamber for 24 hours prior to the start of the experiment to reach equilibrium with the glove box atmosphere.

Aliquots of 150 mL of input solution were dispensed into amber bottles containing 2.50 ± 0.02 g ZVI and individual bottles were capped. Twenty-one 250 mL amber glass bottles (VWR International, Radnor, PA, USA) were used for each set of batch experiments. Duplicate bottles (designated ‘A’ and ‘B’) were randomly selected and sampled simultaneously at each time step to assess reproducibility within the experiment. A control bottle was included in all four batch experiments, which contained the input solutions without ZVI to monitor changes in Zn concentration that were not caused by Zn reacting with the ZVI. Each bottle was sacrificed after sampling (i.e. each bottle had one sampling event).

2.3.2 Water Sampling and Geochemical Analysis

Aqueous samples were collected at various time points throughout the experiment to examine changes in aqueous geochemistry, including pH, redox potential (Eh), alkalinity, cations and anions. All the filtering, sample manipulation and Eh, pH, and alkalinity measurements were completed in the anaerobic glovebox. Measurements of Eh and pH were conducted immediately on unfiltered samples. The pH was measured using an Orion Ross 815600 pH electrode (Thermo Scientific, Waltham, MA, USA) which was calibrated using pH 4, 7, and 10 standard buffers. The Eh was measured using an Orion 9678 electrode which was checked with Zobell's solution (Nordstrom, 1977) and Light's solution (Light, 1972). Samples for alkalinity measurements were filtered using 0.2 μm Supor membrane filters (Acrodisc, Pall, UK) and polyethylene syringes (BD, Franklin Lakes, NJ), alkalinity was determined using bromocresol green-methyl red indicator and a digital titrator (Hach Co., USA) with a 0.16 N H_2SO_4 cartridge. Alkalinity was measured in duplicate, and the average value was recorded for each sample bottle.

Samples were vacuum filtered using 0.45 μm cellulose acetate filters (Whatman, UK), to remove the ZVI particles. Aqueous samples were then filtered using 0.2 μm filters and polyethylene syringes. Samples for cation and isotope analyses were acidified to pH < 2 using concentrated ultra-pure HNO_3 (Omnitrace ultra, EMD Millipore). Cations and S were measured by inductively coupled plasma-optical emission spectrometry (ICP-OES; Thermo Scientific iCAP 6500).

2.3.3 Isotope sample preparation

All sample preparation and purification procedures were conducted in a clean laboratory

environment and under a HEPA-filtered laminar fume hood. Omni trace ultra-nitric acid (VWR) and trace metal grade HCl, which was distilled with a sub-boiling still (Savillex, DST-1000), were used in the purification procedure and for isotope analysis.

Aqueous samples were purified using a modified extraction procedure described by Maréchal et al. (1999) using an anion-exchange resin (AG-MP-1M 100-200 mesh; Bio-Rad, USA) to remove matrix effects and interferences. These include Fe (5 mg L^{-1}) which was released from the ZVI, and can form a polyatomic interference ($^{54}Fe^{16}O^{+}$) with ^{70}Zn and Ca (≈ 4 mg L^{-1}) which was added as $CaCO_3$ to increase the alkalinity in experiments BT3 and BT4.

Before sample purification, the AG-MP-1M resin was washed to remove any contaminants including trace elements. The resin was first washed using a batch technique outlined in Table 2. After washing, the resin was regenerated using 7 M HCl and then 1.6 mL of resin was loaded into 3 mL SPE columns (Supelco, Bellefonte, PA, USA) packed between two 0.2 μm frits (Supelco, Bellefonte, PA, USA). Once loaded onto the column the resin was washed again and then regenerated in 7 M HCl (Table 2).

Table 2 Resin wash and conditioning procedure

Washing solution	Batch Wash/Column Wash
7 M HCl	10 times
2 M HCl	5 times
Milli-Q® ultra-pure water	5 times
0.5 M HNO_3	5 times
7 M HCl	Regeneration/ Condition
Load 1.6 mL resin to each 3 mL SPE columns	
0.5 M HNO_3	12 mL
2 M HCl	12 mL
Milli-Q® ultra-pure water	9 mL
7 M HCl	15 mL
Regeneration/ Condition	

To adjust for fractionation during chemical purification and isotope measurement, 5.92 μg of Zn double spike solution (Isoflex, Sun Francisco, USA; ^{67}Zn:^{70}Zn = 0.43:0.57) was added to 10.08 μg of Zn in the sample (Matthies et al., 2014). The ratio between the double spike and the sample was 0.37, which was calculated using the Double Spike Tool Box (Rudge et al., 2009). Each sample was then evaporated to dryness in clean Teflon vials, the residue was re-dissolved in 1 mL of 7 M HCl and evaporated to dryness. This process was repeated twice, in order to convert sample to Cl^- species which were retained on the ion-exchange resin. The Zn spiked sample residue was dissolved in another 1 mL of 7 M HCl acid and loaded into the SPE column.

In each purification event, spiked samples were purified in duplicate along with one procedural blank and two spiked standard samples. The standard samples used IRMM 3702 standard with the double spike which has a known isotopic composition, the blanks were 1 mL of 5 M HNO3.

Zinc was retained on the resin and interfering matrix elements such as Ni, S, Ca, Mg, Na and Cu were washed from the resin using 28 mL of 7 M HCl, Fe was washed from the resin using 32 mL of 2 M HCl. Finally, Zn was eluted from the resin in 18 mL of 0.5 M HNO_3. Zinc was collected and evaporated to dryness in 30 mL Teflon vials, the residues were dissolved in 5 M HNO_3 and evaporated down twice to convert the chloride species to nitrate prior to MC-ICP-MS. These residues were then dissolved in 1 mL of 5 M HNO_3, and ultra-pure water was then added to the vial to obtain a final HNO_3 concentration of 0.5 M with 1.381 mg L^{-1} Zn. The purified samples were then diluted in 0.5 M HNO_3 to give a final concentration of 0.69 mg L^{-1} prior to MC-ICP-MS. The procedural blank and standards were treated as samples.

2.3.4 Isotope sample measurement

Zinc stable isotopes were measured using a multi-collector inductively-coupled plasma mass spectrometer MC- ICP-MS (Thermo Scientific Neptune) in medium-resolution mode. Samples were introduced by a stable inlet system (double cyclonic spray chamber). Each analytical sequence measured two purified spiked standards, one purified blank and a maximum of 9 spiked samples. One wash blank (0.5 M HNO_3) was bracketed between each sample (standards and blank) to ensure there was no Zn contamination from the wash step. Five Zn stable isotopes (^{64}Zn, ^{66}Zn, ^{67}Zn, ^{68}Zn and ^{70}Zn) were measured simultaneously; additionally, ^{62}Ni and ^{72}Ge were measured at the same time to correct for isobaric interferences on ^{64}Zn and ^{70}Zn. To correct for the isobaric interferences, ^{64}Ni and ^{70}Ge were calculated assuming $^{66/64}$Ni (3.903225806) and $^{70/72}$Ge (0.756717501). Off-center peak was measured to minimize polyatomic interferences. The signal sensitivity of ^{64}Zn was approximately 1.5 V. Integration time was 8.389 s, with 100 cycles per block. A double-nested iteration correction procedure (Siebert et al., 2001) was used to account for analytical isotope fractionation and instrumental mass bias using the double spike technique. Zinc isotopes ratios 67/64 and 70/64 were checked to verify mass-dependent fractionation. The total procedural blanks (purification and mass spectrometry) of Zn contributed an average 0.59% to the total Zn signal.

Each sample and duplicate was measured in three separate analytical events, providing six measurements for each sample to assess the reproducibility. The final results were calculated by averaging and reported as δ^{66}Zn in per mil (‰) relative to the international Zn isotope standard IRMM-3702, where

(4) $$\delta^{66}Zn = \left[\frac{(^{66}Zn/^{64}Zn)_{sample}}{(^{66}Zn/^{64}Zn)_{IRMM-3702}} - 1\right] \times 1000‰$$

To compare isotope ratios in different batch experiments, δ^{66}Zn was reported relative to $^{66}Zn/^{64}Zn$ of its input solution, where

(5) $$\delta^{66}Zn = \left[\frac{(^{66}Zn/^{64}Zn)_{sample}}{(^{66}Zn/^{64}Zn)_{input\ solution}} - 1\right] \times 1000‰$$

The fractionation factors, represented as α, were achieved by fitting experimental δ^{66}Zn results to Rayleigh distillation models (Clark and Fritz, 1997):

(6) $$\frac{R}{R_0} = f^{(\alpha-1)}$$

Where R is the isotope ratio, f is the fraction of Zn (II) remaining in solution. In Equation 6, α represents the fractionation factors of the solution ($\alpha_{ZVI\text{-}solution}$). In addition, the experimental δ^{66}Zn results were fitted using an equilibrium model, fractionation factors which represent the isotope fractionation in solution can be expressed using Equation 7 (Balistrieri et al., 2008; Juillot et al., 2008):

(7) $$\delta^{66}Zn = \frac{(1-f)\times(\alpha-1)}{(1-f)+\alpha f} \times 1000‰$$

Where f is the same as in Equation 6, representing the Zn (II) fraction remaining in solution. However, in Equation 7, α represents the fraction from solution phase to solid phase.

Isotope fractionation value (ε) was introduced by Coplen et al., (2011) and expressed as per mil:

(8) $$\varepsilon = (\alpha - 1) \times 1000‰$$

Separation factor, which has been used in previous Zn isotope studies (Cacaly et al., 2004; Pokrovsky et al., 2005; Balistrieri et al., 2008; and Juillot et al., 2008), is described as:

(9) $$\Delta_{solution-ZVI} = \delta^{66}Zn_{solution} - \delta^{66}Zn_{ZVI}$$

2.3.5 Solid-phase data collection and analysis

Following the method of Jamieson-Hanes et al. (2012) and Shrimpton et al. (2015), samples were vacuum filtered using a 0.45 μm cellulose acetate filter to separate ZVI in the anaerobic chamber. Solid samples were transferred to and stored in glass vessels, which were sealed with electrical tape and wrapped with several layers of zip lock bags to keep them anaerobic. Subsequently, solid samples were removed from the anaerobic chamber and frozen by immersion in liquid nitrogen. Frozen samples were then freeze dried (Labconco FreeZone, Kansas City, MO, USA). Once completely dry samples were stored in an anaerobic chamber for future analysis.

Synchrotron-based X-ray absorption near edge structure (XANES) and extended X-ray absorption fine structure (EXAFS) techniques were used at XSD beamline 20-BM-B at the Advanced Photon Source, Argonne National Laboratory (Chicago, IL, USA). XANES can be used to identify the oxidation states of Zn on the reactive media, and EXAFS can provide information about the coordination environment, and also the local structure of Zn. Because the batch experiments were performed over a relatively short time (11 days), and the input solution had a low concentration of Zn (5 mg L^{-1}) and 2.5 g of ZVI, only the sample taken at the last time point was selected from each experiment for the XANES study. Samples that were used for EXAFS are required to have a greater concentration of Zn and in particular a higher Zn/ Fe ratio, in order to reduce the interference of Fe on the Zn signal.

Additional batch experiments were conducted to accumulate a greater concentration of Zn on the ZVI. In these experiments, 150 mL of input solution containing 5 mg L^{-1} of Zn was reacted with 2.5 g of ZVI, the input solution was replaced every 5 days and this process repeated.

Freeze dried samples collected from these batch experiments were packed separately in 0.5 mm-thick and 1 mm^2 acrylic sample holders and sealed using Kapton® tape in an anaerobic chamber. An anaerobic container was used to transfer samples from the University of Waterloo to APS. Reference materials (i.e. Zn foil) were scanned simultaneously with bulk samples for normalization in transmission mode while bulk samples were scanned in fluorescence mode. Aluminum foil was overlaid onto the detector during sample scanning to reduce the interference from the Fe signal. Up to 20 replicate scans were aligned, deglitched, merged and normalized before linear combination fitting was conducted on the merged scans. The data processing was completed with the program ATHENA, which is a component of the IFEFFIT software package (Ravel and Newville 2005).

Athena and WinXAS were used for data reduction and R space curve fitting, respectively. The amplitude of $\chi(k)$ damped quickly at high k because of static and thermal disorders, however, the amplitude of $\chi(k)$ at high energy includes significant information regarding structure; thus k^3-weighted results were used to emphasize the oscillations. Fourier transformed $k^3\chi(k)$ spectra used a Gaussian window with a window parameter of 30 to obtain radial distribution functions (RDFs).

Theoretical calculation was processed using FEFF 7, based on the crystal structural information from the American Mineralogist Crystal Structure Database. The structural information of each shell was determined including phase-shift and scattering amplitude functions. The Fourier filtered experimental spectra from this study were least-squares fitted with the theoretical function using WinXAS providing the structural information (i.e. coordination number, distance between Zn and nearest atoms and Debye-Waller factor).

The process of EXAFS modeling was included in the following flow chart (Figure 1):

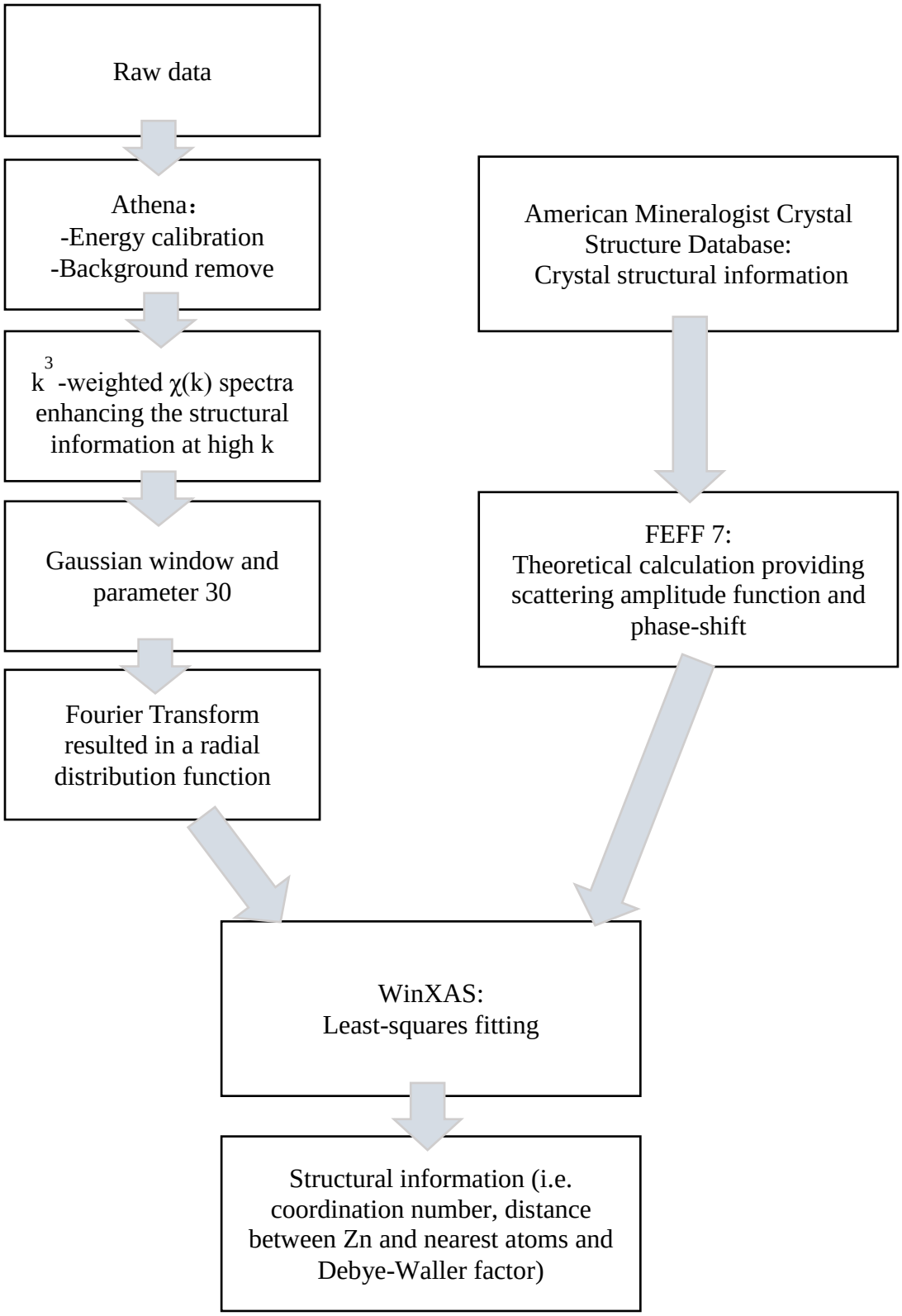

Figure 1 EXAFS modeling flow chart

The magnitude of the Fourier Transformed spectra, and the imaginary part of Fourier Transform spectra, were compared for each of the experimental spectra. Further comparisons were made by fitting the residual of the magnitude of Fourier Transform for the whole R region, the Fourier Transform at the second-shell R region and the imaginary part of Fourier Transform at the second shell region.

2.3.6 Geochemical Modeling

Aqueous geochemical data was used to provide input to PHREEQC (version 3) (Parkhurst and Appelo 2013) with the WATEQ4f thermodynamic database to simulate the batch experiments and determine the thermodynamic stability of solid phases. In every batch experiment, a sample collected from each different time point was considered as an isolated input solution, and the calculation results were used to interpret the Zn precipitates in the solid phase co-existing with the solution at the different time points. The results were expressed as the saturation index values, where

(10) $$SI = \log IAP - \log K$$

In equation 10, IAP is defined as the ion activity product and K is defined as the solubility constant. A positive SI value indicates the solution is supersaturated with respect to the target mineral. An SI value of 0 indicates that equilibrium has been attained. When the SI value is less than 0, the solution is unsaturated with respect to the mineral.

2.4 Results and Discussion

2.4.1 Geochemical analysis

The initial pH of the solution in BT1 was 6.41. The pH dropped to 5.92 after one hour and kept dropping to 5.37 after four hours. The pH of samples collected at the eighth hour was increased back to 6.42, and the pH was kept increasing after eight hours. The pH increased rapidly in the time period between 8 hours to 48 hours and then changed less rapidly for the remainder of the experiment (Figure 2, BT1).

In BT2, the initial pH of the input solution was 5.81. The pH of the samples collected at the eighth hour was dropped to 2.97 in replicate A and to 3.53 in replicate B. The pH stayed lower than before 24 hours, and after 24 hours, the pH was increasing over time (Figure 2, BT2).

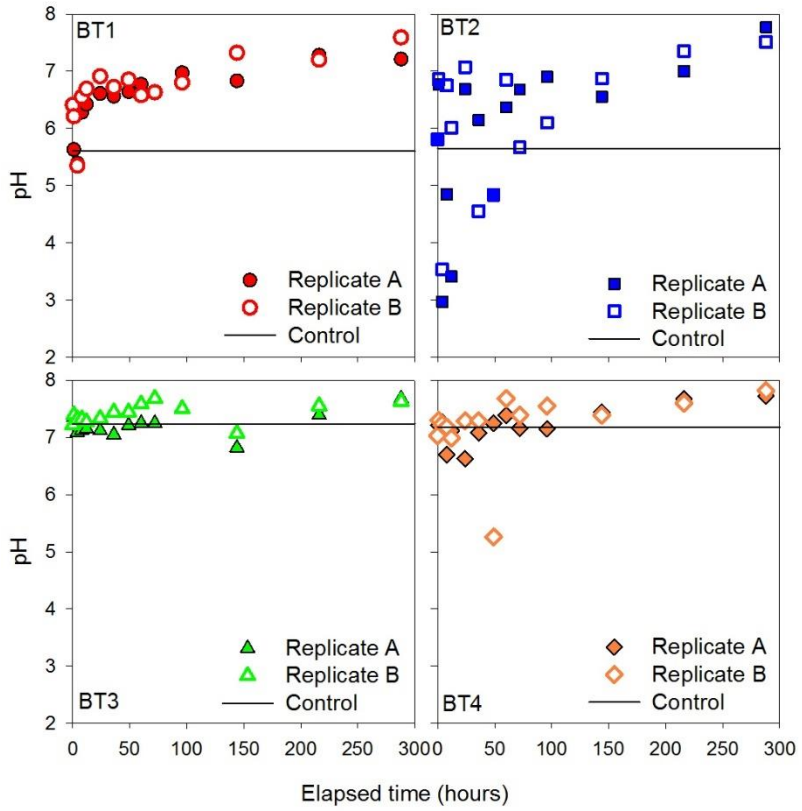

Figure 2 Change in pH as a function of time in the batch experiments. The solid line shows the pH of ZVI-free Zn stock input solution control.

Despite the similar general trend in pH over time in the ultra-pure water systems (BT1 and BT2), there was variability in the pH measurements between duplicate experiments (Figure 2), especially at the earlier sampling times. Although the duplicates were set up and measured under the same conditions, the reactions occurred in separate independent bottles.

Two major reactions could control the differences in pH between replicates observed in these experiments. The reduction of H_2O and the oxidation of Fe can increase pH (Equation 11), and this reaction is a characteristic of ZVI corrosion under anaerobic conditions (Lindsay et al. 2008):

(11) $$2H_2O + Fe^0\,(s) \rightarrow Fe^{2+} + 2OH^- + H_2\,(aq)$$

If O_2 was entrained in ZVI/H_2O, the oxidation of Fe^{2+} by dissolved O_2 could produce H^+ (Equation 12) and decrease the pH (Lindsay et al. 2008):

(12) $$O_2 + 10\ H_2O + 4\ Fe^{2+} \rightarrow 4Fe(OH)_3 + 8H^+$$

If the reaction described in Equation 11 was the only reaction occurring, the concentration of dissolved Fe would gradually increase; however, in the first 48 hours, Fe(aq) concentrations varied over time (Figure 3). The pH fluctuates downward with a decreasing Fe concentration at the beginning of the experiment. This observation suggests that precipitation of $Fe(OH)_3$, subsequently removed during filtration resulted in the low Fe concentration and low pH. Therefore, the samples which had low Fe concentration and low pH were likely caused by the reaction described in Equation 12.

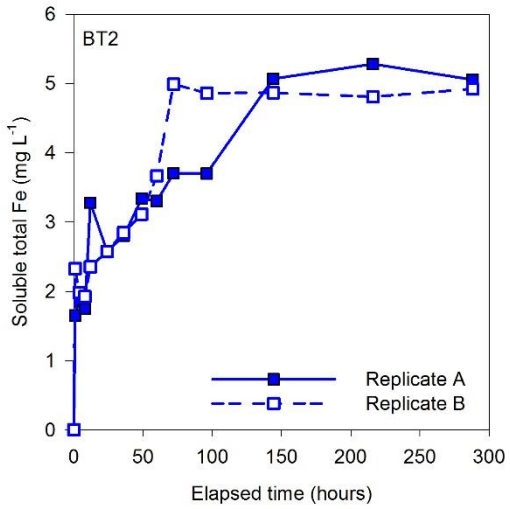

Figure 3 Concentration of Fe change as a function of time in BT2. In the beginning of experiments, the concentration of Fe fluctuates causing a difference between replicate samples.

With no alkalinity to buffer changes in the pH, the pH in the ultra-pure water systems BT2 were sensitive to the presence of traces of O_2. Oxygen entrapment may have affected the early time points. The pH of the solution was lower than the initial pH during the initial 4-24 hours after the initiation of the experiment, and the duplicates were inconsistent until 150 hours. After

150 hours, the pH became more stable than during the initial period (0-48 hours), the pH between duplicates was more consistent, and the pH values were similar to those from the other experiments.

In BT2, the samples from the early time period (4 hours to 24 hours) had the pH within 2-4. The low pH suggested the anaerobic environment of BT2 was changed by oxygen, and the mechanisms which removed Zn might be changed. According to Equation 12 and Figure 3, in BT2, during the initial 12-24 hours, the ferrous iron in the solution formed $Fe(OH)_3$, which is an active sorbate for Zn(II). In addition, the acid environment inhibits the formation of Zn precipitation. The reaction condition of BT2 was different from the other batch experiments. Except the low pH, the influence of the trapped oxygen in BT2 had uncertain influence on other geochemical results, isotope results, or solid phase results. Therefore, in the following discussion, the collected data of BT2 were processed the same as the other three batch experiments, but it will be discussed separately.

The pH was less variable in the system which contained $CaCO_3$ (BT3 and BT4). In BT3, the pH increased from 7.22 to 7.65 over 288 hours, and the pH increased from 7.03 to 7.77 in BT4. The pH change was buffered by the alkalinity, thus the duplicates were more consistent and only one measurement of pH (replicate B, experiment BT4 at 48 h) was lower than the overall trend.

The input solutions of the four batch experiments had Eh values ranging from 370 to 460 mV. (Figure 4). In all of the experiments the Eh decreased over time, and after 288 hours, the Eh values were between 0 to -250 mV. These observations suggest that the experimental conditions changed from oxic to weakly reducing over time. The increase in alkalinity did not affect the Eh measurements. There was some variability in the Eh measurements between replicates which may have been due to the low concentrations of redox active elements. The Eh cannot be

measured accurately by Eh probe in solutions with weak exchange currents (Lindberg & Runnells, 1984). Also, the increasing ferrous iron in solutions may yield unstable readings (Nordstrom & Wilde, 2005); thus, scattered between data points appeared at later times.

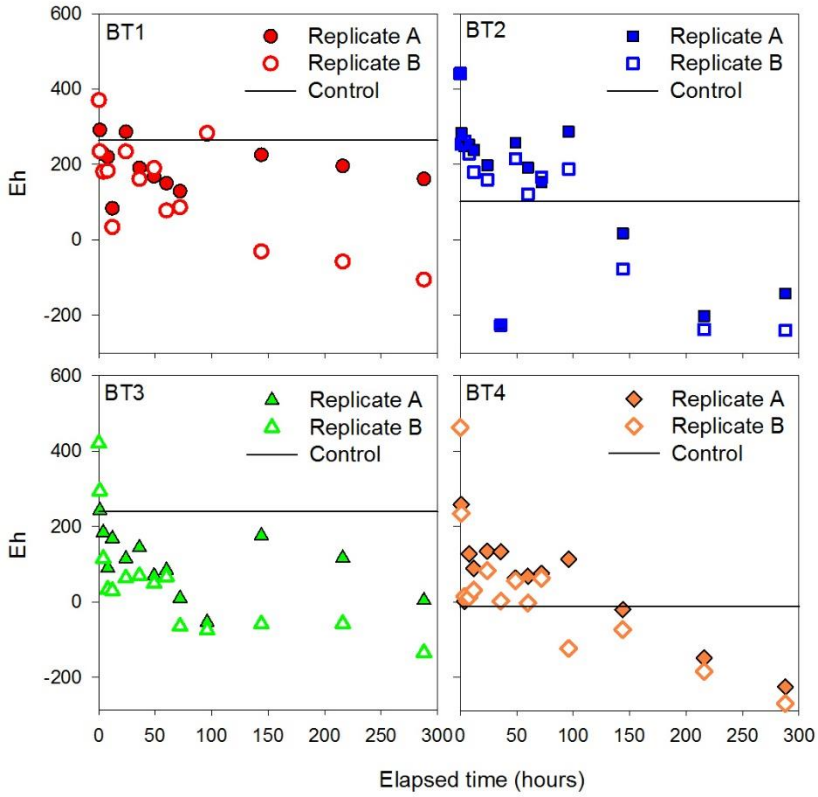

Figure 4 Eh change as a function of time in all batch experiments.

In the system, with $CaCO_3$ (BT3 and BT4) the alkalinity of the input solutions was 6 mg L^{-1} (as $CaCO_3$) and remained constant throughout the experiment. In the ultra-high purity water experiments (BT1 and BT2), the alkalinity was stable during the entire experiment and lower at < 0.2 to 2 mg L^{-1} as $CaCO_3$ due to the absence of $CaCO_3$ in the input solution.

The concentration of Ca remained constant over time in BT3 and BT4 approximately 4 mg L^{-1} indicating that Ca was not removed through reactions with the ZVI and that no Ca was released from the ZVI. In the control experiments $Fe_{(aq)}$ remained below ICP-OES quantification

limit of 200 μg L^{-1} over time; however, in all of the experiment samples containing ZVI, there was an increase in $Fe_{(aq)}$ reaching a maximum of 5 mg L^{-1} suggesting that Fe in solution was released from the ZVI. Other dissolved metals the input solution, samples and controls were below the ICP-OES quantification limit of 200 μg L^{-1}, demonstrating that the acid washed ZVI did not release significant concentrations of other elements.

2.4.2 Zinc removal

In the initial stages of all of the experiments Zn was rapidly removed from solution (Figure 5). The reaction rate slowed over time, and after 216 hours the concentration of Zn did not decrease by more than 5% of the input Zn concentration. At the end of the experiment (288 h) the concentration of unreacted Zn decreased from 5 mg L^{-1} to < 0.2 mg $L^{-1.}$ Because the Zn concentrations in the initial solutions of the four batch experiments were differed, the fraction of Zn remaining in solution (*f* in Figure 5) was used to compare Zn removal across the experiments. At the end of experiments, 98%, 95%, 97% and 98% aqueous Zn was removed in BT1, BT2, BT3 and BT4, respectively.

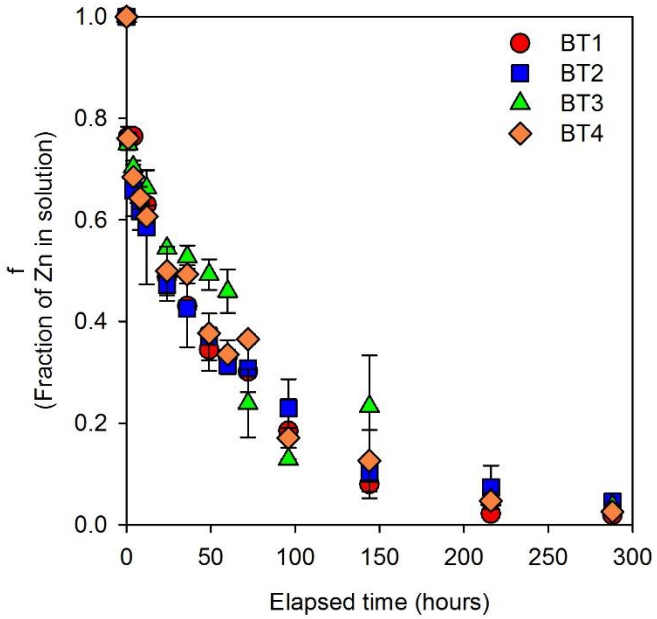

Figure 5 Fraction of Zn in solution (*f*) as a function of time in all batch experiments. The error bars represent the σ uncertainty due to duplication of the samples.

The $Zn_{(aq)}$ concentrations in the ZVI free controls did not change significantly over time which suggests that Zn removal was due to attenuation/reaction with the ZVI rather than precipitation from solution or loss to the vessel walls. Despite the differences in the pH and Eh between replicates, the Zn concentration was reproducible.

Duplicate samples collected at 12 hours in BT2 and at 96 hours in BT3 had standard deviation values (σ) approximately equal to 0.1, while others had smaller standard deviation of *f* value which is less than 0.1. Among the 56 samples, only two sample pairs (duplicates collected at 12 hours in BT2 and duplicates collected at 96 hours in BT3) had larger standard deviation values (σ) (around 0.1) of *f* values. The variations between these duplicates may be caused by the differences in the surface area of the ZVI in the reaction vessels. The surface area would influence the reaction rate (Wilkin and McNeil, 2003) and contribute to the variability in Zn concentration between duplicates observed here.

Zinc removal rates were modeled using a pseudo-first-order equation (Wilkin and McNeil 2003) (Figure 6), as:

(13) $$\frac{\mathrm{d[Me]}}{\mathrm{dt}} = -k_{obs}[M_e]$$

Where M_e represents the molar concentration of Zn, k_{obs} is the rate coefficient, and t is elapsed time in hours. With the measured input concentration of Zn (II) (M_e^0), the equation can be integrated to:

(14) $$\ln(M_e) - \ln(M_e^0) = -k_{obs} \times t$$

and,

(15) $$\mathrm{f} = e^{-k_{obs} \times t}$$

The rate coefficients in different batch experiments were calculated and listed in Table 3, and the R^2 values, also listed in Table 3, show the pseudo-first order model fit for the experimental data.

Table 3 Zn removal rate coefficients and fitting R^2 calculated by pseudo-first order model for all batch experiments

k_{obs} (h^{-1})	BT1	BT2	BT3	BT4
	0.0234± 0.0037	0.0238± 0.0047	0.0186± 0.0036	0.0214± 0.004
R^2	0.9217	0.7553	0.8216	0.8930

A t-test was applied to compare the reaction rate of four batch experiments; p-values of T-test was given in Table 4:

Table 4 p-value of T test for Zn removal rate coefficient comparison in different batch experiments

p-value	BT1/BT2	BT1/BT3	BT1/BT4	BT2/BT3	BT2/BT4	BT3/BT4
	0.9766	0.7675	0.9333	0.7348	0.9063	0.8274

According to the results of the t-test of k_{obs}, the reaction rates of four batch experiments were not significantly different ($p > 0.05$; Table 4). the variation of all four k_{obs} (0.0024) is smaller than the standard deviation of each k_{obs}. These reaction rates indicate that, within the concentration range of the initial solutions ($ZnCl_2$ or $ZnSO_4$) and the changes in alkalinity, the rates of Zn removal are consistent. In addition, the reaction rate in the different batch experiments was controlled by the availability of ZVI surface area (Johnson et al., 1996). Thus, the specific reaction rate of Zn removal can be normalized to ZVI surface area using,

(16) $$k_{sa} = \frac{k_{obs}}{a_s \times \rho_m}$$

Where a is the specific surface area of ZVI, and ρ_m is the concentration of ZVI in the batch experiment (16.67 g L^{-1}). A specific surface area of the ZVI was 2.8306 ± 0.0059 m^2 g^{-1}, was determined using the Brunauer-Emmett-Teller (BET) method. Similar k_{SA} values are observed in Table 5.

Table 5 Specific surface area normalized Zn removal reaction rate

k_{SA} (mL h^{-1} m^{-2})	BT1	BT2	BT3	BT4
	0.50± 0.08	0.50± 0.10	0.39± 0.08	0.45± 0.08

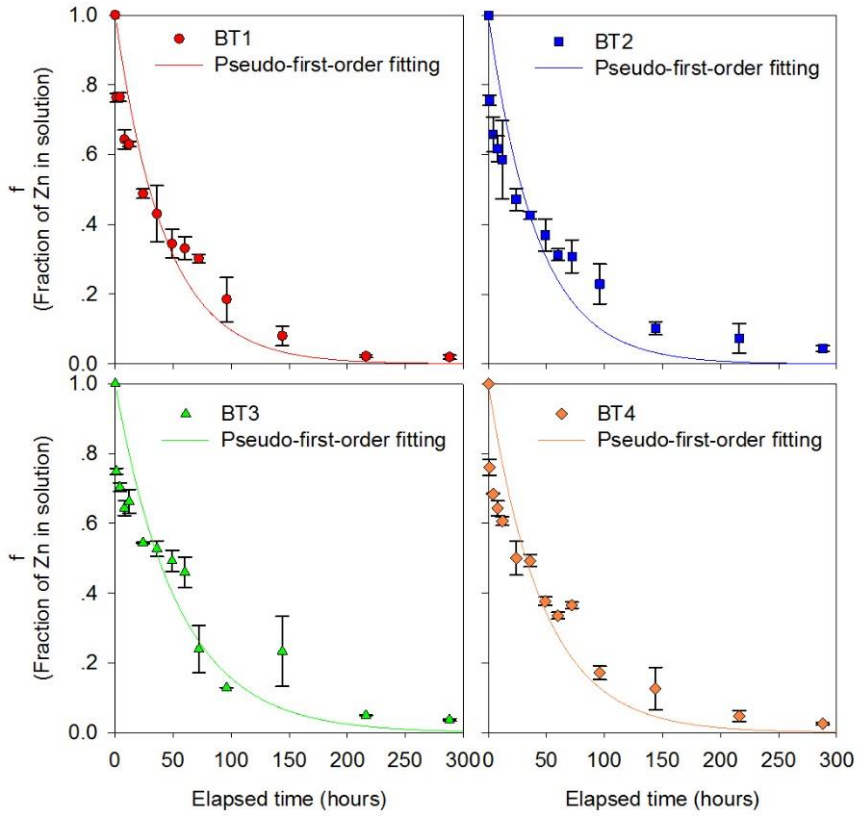

Figure 6 Pseudo-first order model was used to fit the measured fraction of Zn in solution (f) as a function of time (elapsed time). Zinc removal rate coefficients for all batch experiments can be given as a parameter by this fitting. The error bars σ represent the variations determined from duplicate samples.

2.4.3 Modeling of geochemical data

Geochemical modeling of each of the separate batch experiments (including replicates) was conducted using PHREEQC to understand (a) the speciation of Zn in the input solutions, (b) the aqueous Zn species during the experiment and (c) to determine thermodynamically stable solid phases and likely precipitates.

In the low alkalinity batch experiments (BT1 and BT2), regardless of which salt was used for the Zn input solution and the influence of oxygen in BT2, the calculation indicated that more than 97% of the Zn in solution was free Zn^{2+} (Table 6). At the end of batch experiments (288

hours), the fraction of $Zn^{2+}_{(aq)}$ had decreased, but was still predominant. The contribution of $ZnHCO_3^+$, $ZnOH^+$, and $Zn(OH)_2$ increased slightly over time but accounted for < 5% of the total aqueous species.

Table 6 Fraction of Zn species in the input and 288 hrs solution of BT1 and BT2

	BT1 replicate A		BT1 replicate B		BT2 replicate A		BT2 replicate B	
	0	288	0	288	0	288	0	288
Zn^{2+}	97.83	94.98	99.25	93.35	99.42	87.02	99.42	92.89
$ZnSO_4$	1.36	1.32	0.47	1.27	0	0	0	0
$ZnHCO_3^+$	0.45	0.84	0	0	0.48	0.77	0.48	0.84
$ZnOH^+$	0.26	1.59	0.27	3.77	0.07	5.34	0.07	3.13
$ZnCO_3$	0.08	0.99	0	0	0.02	3.31	0.02	1.99
$Zn(OH)_2$	0.01	0.29	0.01	1.65	0	3.55	0	1.14

Zinc (II) accommodates six water molecules with an octahedral structure forming $Zn(H_2O)_6^{2+}$ (Kuzmin et al., 1999), thus most of Zn in the solution of BT1 and BT2 occurred in an octahedral structure with a coordination number of 6. The increase in $ZnHCO_3^+$, $ZnOH^+$ and $Zn(OH)_2$ would not significantly contribute to the overall coordination environment of Zn in solution. Although the dominant coordination number of Zn in the aqueous phase did not change over time, the coordination number of Zn in solid phase may have changed.

The solutions of BT1 and BT2 were supersaturated with respect to $Fe(OH)_3$, goethite (FeOOH) and hematite (Fe_2O_3) and undersaturated with respect to siderite ($FeCO_3$), smithsonite ($ZnCO_3$), sphalerite (ZnS), and $Zn(OH)_2$.

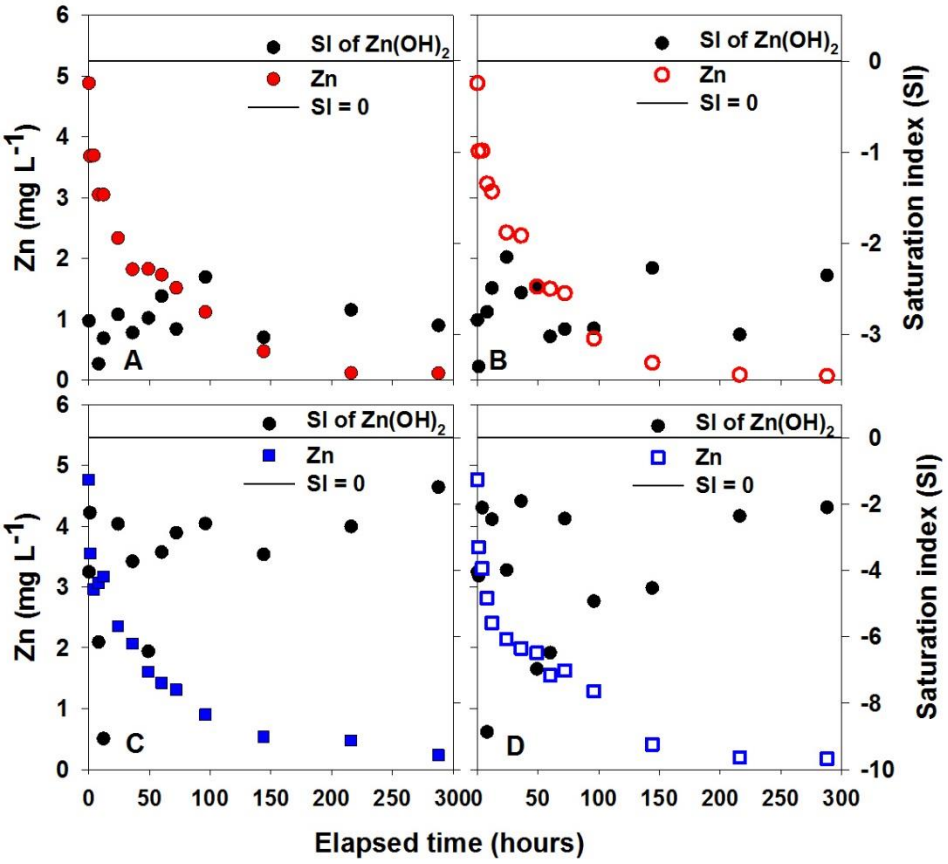

Figure 7 Concentrations and PHREEQC predicted saturated index of dissolved Zn as a function of time. A: BT1 replication A; B: BT1 replication B; C: BT2 replication A; D: BT2 replication B.

Dissolved Zn concentration and PHREEQC predicted saturated index (SI) of $Zn(OH)_2$ was plotted as a function of time in Figure 7. The solutions of BT1 and BT2 were undersaturated with respect to $Zn(OH)_2$. The predicted SI values of $Zn(OH)_2$ in BT1 replicated A and replicated B were within the range of -2 to -3.5. The predicted SI values of $Zn(OH)_2$ in BT2 were within a range of -1.5 to -9.5, and the time points where had lower pH had more negative SI values of $Zn(OH)_2$ (Figure 8), indicating the oxygen trapped in BT2 reduced the pH and inhibited the formation of Zn precipitation ($Zn(OH)_2$)

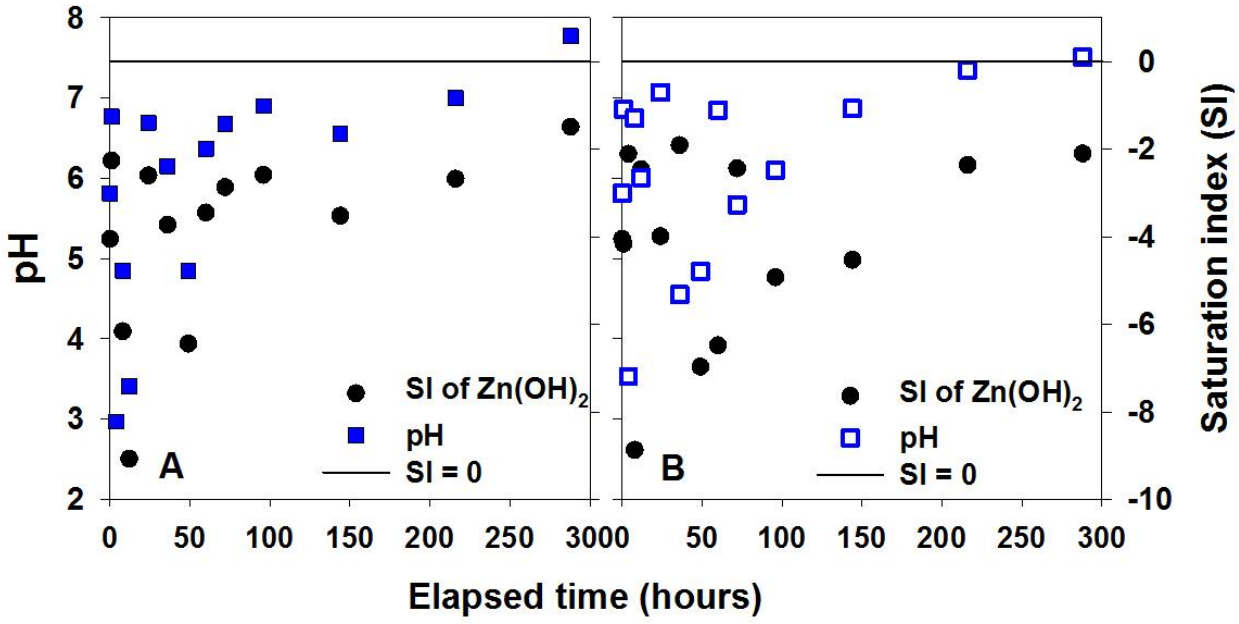

Figure 8 PHREEQC predicted SI of Zn(OH)2 and pH of the solutions in BT2 as a function of reaction time. A: BT2 replication A, B: BT2 replication B.

In the higher alkalinity experiments (BT3 and BT4), total soluble Zn concentration in the input solutions was similar to lower alkalinity batch experiments. However, the Zn (aq) species in the input solution were dominated by the $Zn(OH)_{2\,(aq)}$ species. The concentration of the four most abundant soluble Zn species ($Zn(OH)_2$, Zn^{2+}, $Zn(OH)^+$ and $ZnCO_3$) are listed in Table 7.

Table 7 Concentrations of the four most abundant soluble Zn species in BT3 and BT4, calculated by PHREEQC

Time (h)	BT3 Replicate A (mg/L)				BT3 Replicate B (mg/L)				BT4 Replicate A (mg/L)				BT4 Replicate B (mg/L)			
	Zn^{2+}	$Zn(OH)_2$	$Zn(OH)^+$	$ZnCO_3$	Zn^{2+}	$Zn(OH)_2$	$Zn(OH)^+$	$ZnCO_3$	Zn^{2+}	$Zn(OH)_2$	$Zn(OH)^+$	$ZnCO_3$	Zn^{2+}	$Zn(OH)_2$	$Zn(OH)^+$	$ZnCO_3$
0	4.86	2.31	0.60	0.23	4.86	2.31	0.60	0.23	4.50	2.01	0.57	0.18	4.50	2.01	0.57	0.18
1	3.67	2.99	0.28	0.11	3.61	3.27	0.17	0.06	3.35	1.53	0.42	0.13	3.49	1.63	0.44	0.14
4	3.38	1.18	0.41	0.16	3.46	2.76	0.28	0.11	3.07	1.68	0.37	0.11	3.08	1.60	0.38	0.12
8	3.05	2.06	0.32	0.12	3.20	1.15	0.39	0.15	2.83	0.75	0.34	0.11	2.96	1.18	0.37	0.11
12	3.34	2.68	0.26	0.10	3.10	2.11	0.32	0.12	2.69	1.30	0.34	0.10	2.77	1.02	0.35	0.11
24	2.65	0.07	0.12	0.05	2.64	1.81	0.27	0.11	2.09	1.39	0.23	0.07	2.40	1.15	0.30	0.09
36	2.64	0.29	0.23	0.09	2.48	2.27	0.10	0.04	2.27	0.57	0.27	0.08	2.16	1.52	0.22	0.07
49	2.29	1.92	0.15	0.06	2.50	2.09	0.17	0.07	1.66	0.32	0.18	0.06	1.73	1.12	0.19	0.06
60	2.38	2.01	0.16	0.06	2.09	1.92	0.08	0.03	1.54	0.74	0.19	0.06	1.48	0.76	0.18	0.06
72	1.39	1.21	0.08	0.03	0.63	0.60	0.01	0.00	1.61	0.45	0.19	0.06	1.67	0.23	0.16	0.05
96	0.63	0.55	0.04	0.01	0.93	0.86	0.04	0.01	0.83	0.11	0.08	0.02	0.71	0.55	0.06	0.02
144	0.83	0.05	0.06	0.05	1.55	1.05	0.15	0.11	0.38	0.19	0.04	0.03	0.78	0.40	0.09	0.07
216	0.25	0.04	0.02	0.02	0.26	0.16	0.03	0.02	0.16	0.07	0.02	0.02	0.27	0.20	0.02	0.02
288	0.18	0.09	0.02	0.02	0.20	0.16	0.01	0.01	0.11	0.10	0.00	0.00	0.13	0.12	0.00	0.00

In the solid phase, Zn bonds with oxygen in $Zn(OH)_2$ with a tetrahedral geometry (Mokili et al., 1996); however, aqueous hydrolysis Zn species (e.g. $Zn(OH)(H_2O)^{5+}$, $Zn(OH)_2(H_2O)_4^0$) commonly have octahedral coordination (Barak & Helmke,1993). Zinc in $ZnCO_3$ adopts an octahedral structure with a coordination number of six (Brown, 2014). The dominant dissolved Zn species varied over time. However, the concentration of $Zn(OH)_2$ and Zn^{2+} was much greater than other species during the experiments. In addition, in the input solutions, $Zn(OH)_2$ and Zn^{2+} have comparable concentrations, and $Zn(OH)_{2\,(aq)}$ became more dominant at the end of the experiments. In a summary, soluble Zn in the input solution occurred as aqueous species with a coordination number of six. Despite the difference in soluble Zn species ($ZnSO_4$ and $ZnCl_2$), aqueous Zn in the ultra-pure water system and the higher alkalinity system have the same coordination number of six.

Experimental solutions from BT3 and BT4 were supersaturated with respect to $Fe(OH)_3$, goethite (FeOOH) and hematite (Fe_2O_3), these minerals had higher SI values in the higher alkalinity experiments. For example, solutions were undersaturated with respect to siderite ($FeCO_3$) in BT1 and BT2, whereas solutions in BT3 and BT4, were slightly supersaturated with respect to siderite ($FeCO_3$) with low SI values ($0 < SI < 2$). Early in the experiment the solutions of BT3 and BT4 were slightly supersaturated with respect to $Zn(OH)_2$ with low SI values ($0 < SI < 2$) and later in the experiment undersaturation with respect to $Zn(OH)_2$ was observed (Figure 9). The solutions in BT3 and BT4 remained undersaturated with respect to smithsonite (ZnCO3), sphalerite (ZnS), and other Zn-containing minerals.

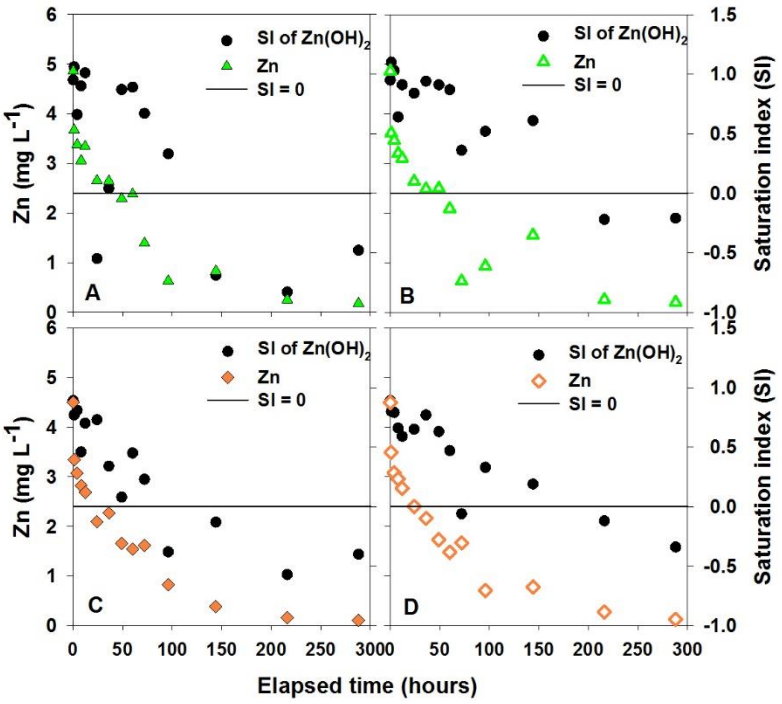

Figure 9 Concentrations and PHREEQC predicted saturated index of dissolved Zn as a function of time. A: BT3 replication A; B: BT3 replication B; C: BT4 replication A; D: BT4 replication B.

Geochemical modeling (PHREEQC) was used to identify the Zn species as a function of time in order to understand the potential Zn removal mechanisms. Formation of metallic Zn or sphalerite would not be favoured under the weakly reducing conditions prevalent in all four batch experiments. According to the results of the modeling, there is no tendency for precipitation of smithsonite ($ZnCO_3$) or $Zn(OH)_2$ in BT1 and BT2. Combining the modeling results and the pH measurement of BT3 and BT4, precipitation of zinc hydroxide $Zn(OH)_2$ is favoured at pH> 7.2. and precipitation of $ZnCO_3$ was not favoured under these conditions. This observation was consistent with previous work by Gélabert et al. (2006), who stated that the precipitation of $Zn(OH)_2$ was more rapid than $ZnCO_3$ precipitation under the similar conditions. Thus, the decreasing concentration of Zn in BT1 is likely caused by Zn adsorption onto surface of Fe (oxy) hydroxides. In BT2, the reaction between oxygen and ferrous iron produced $Fe(OH)_3$;

thus, the reducing Zn concentration in solution is likely caused by Zn adsorption onto Fe(OH)3. In BT3 and BT4, Zn may be removed by either adsorption, similar to the ultra-pure water system, or by precipitation of $Zn(OH)_2$.

In all four of the batch experiments, the concentration of aqueous Zn decreased from nearly 5 mg L^{-1} to 0.1 mg L^{-1}, and the pH increased from nearly 6 to 8. This pH range is an optimum pH for aqueous Zn adsorption to amorphous Fe(III) oxyhydroxide (Balistrieri et al. 2008), goethite and 2-Line ferrihydrite (Juillot et al. 2011). Pokrovsky et al. (2005) reported that Zn was rapidly adsorbed to the surface of Fe minerals when the pH was between 6 and 7; Balistrieri et al. (2008) found that above pH 4.5, Zn was adsorbed onto amorphous Fe precipitates; in addition, adsorption of Zn onto amorphous iron is negligible at pH <5, and most extensive at pH 7 to 8. Juillot et al. (2008) also reported Zn adsorption onto 2-line ferrihydrite at the pH of approximately 6 to 8, and significant adsorption to goethite at pH range of 4 to 8.

Thus these results suggest that the most probable removal mechanisms occurring in these experiments is either the precipitation of $Zn(OH)_2$ and/or Zn adsorption onto coatings on the ZVI or co-precipitation.

2.4.4 Solid-phase Characterization

Input solutions of all batch experiments and untreated ZVI (control) were studied using X-ray absorption near edge structure technology (XANES). Samples (after 288 hours of treatment) of four batch experiments were examined using extended X-ray adsorption fine structure technology (EXAFS). Both Zn and Fe were studied using the samples that were reacted for 288 hours; however, because Fe^0 was the majority of ZVI, and only a thin layer surrounding of ZVI was reacted with the Zn (II) solutions, the EXAFS spectra showed the structural

information of the Fe^0 rather than the reacted Fe. Thus, the structural information regarding the thin coating of reacted Fe, used in the following EXAFS fitting and discussion, was based on previous research.

2.4.4.1 XANES and Linear Combination Results

XANES spectra of all of the batch experiments and standards are shown in Figure 10. Compared to Zn^0 oxidation state, the Zn K-edge position of Zn^{2+} is shifted to a higher energy. The Zn K-edge positions of all batch experiments were consistent with the Zn (II) oxidation state.

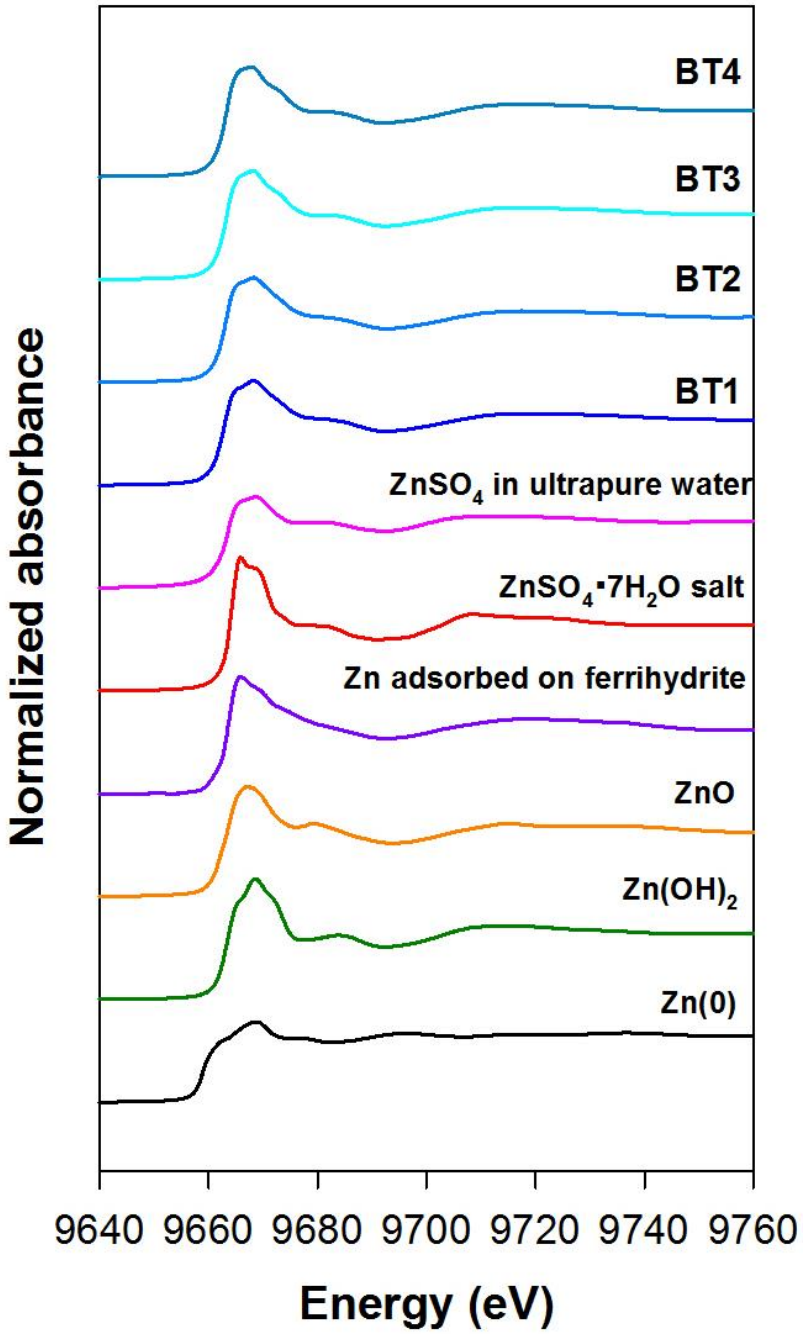

Figure 10 XANES spectra (9640 eV to 9760 eV) for batch experiments and standards.

Linear combination fitting (LCF) was performed to compare the similarity between the

batch experiment samples and a series of standards [including Zn^0, $ZnSO_4$ in ultra-pure water, $ZnSO_4$ salt, Zn adsorbed onto ferrihydrite, ZnO and $Zn(OH)_2$. Table 8 summarizes the contribution of the standards to the sample XANES spectra, and the combination percentage is shown in Figure 11. In BT1, ZnO is the dominant Zn species in the solid phase (71.2 %) and the second most abundant Zn phases are $Zn(OH)_2$ and Zn adsorbed onto ferrihydrite. In BT2, both ZnO and Zn adsorbed onto ferrihydrite are the dominant Zn species in the solid, and $Zn(OH)_2$ is the less abundant species. Compared to BT1, there is more Zn adsorbed onto solid phase than Zn precipitation. In BT3 and BT4, Zn adsorbed onto ferrihydrite is the dominant species, while ZnO and $Zn(OH)_2$ are the less abundant species.

Table 8 Linear composition fitting (LCF) results of all batch experiments

	BT1	BT2	BT3	BT4
Zn adsorbed on ferrihydrite (%)	16.4	33.5	40.5	42.8
$Zn(OH)_2$ (%)	11.1	16.5	27.4	21.6
ZnO (%)	71.2	47.6	30.1	34.4
$ZnSO_4 \cdot 7H_2O$ (%)	0	0	0	0
$ZnSO_4$ in ultrapure water (%)	0	0	0	0
Zn(0) (%)	0	0	0	0
Reduced χ^2	0.00166	0.00087	0.00058	0.00077

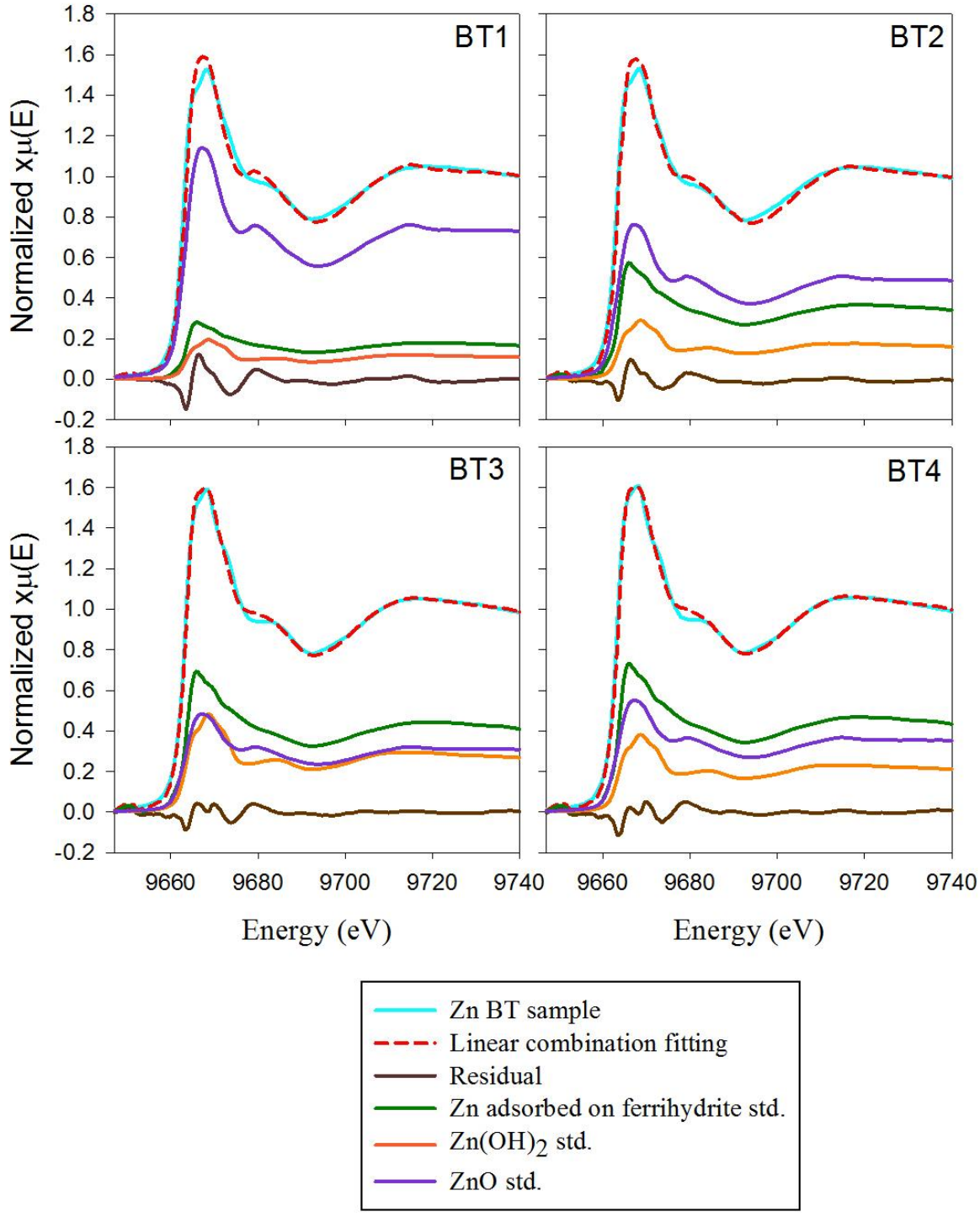

Figure 11 Bulk XANES spectra of Zn for last time point of ZVI samples. Reference standards include Zn adsorbed onto ferrihydrite, $Zn(OH)_2$ and ZnO. The linear combination fitting energy range is (-20eV, 74.012eV) relative to the peak energy.

2.4.4.2 EXAFS fitting results

The oscillations at high k values include significant information regarding the atomic structure, thus k^3-weighting was used to magnify the signal of $\chi(k)$ at high k values and avoiding the attenuation and dampening which is caused by static noise and thermal disorders. Gaussian window, with a window parameter of 30, was used as a window function during Fourier Transform (FT) into R-space.

To have a clear comparison, spectra were plotted to show the differences between the different Zn salts and different alkalinity environments. In k-space (Figure 12), the spectra of all four batch experiments had a similar frequency of oscillations which suggest that the distance between Zn and the first shell atom (Zn-O) in the four batch experiments was similar.

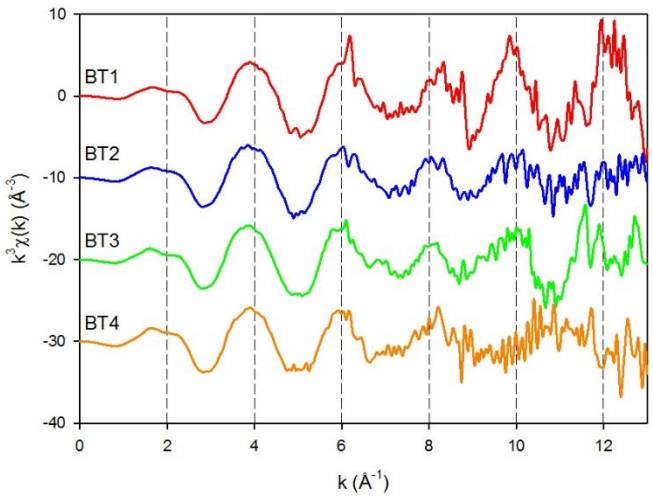

Figure 12 Experimental EXAFS spectra of all batch experiments in k-space with k^3-weight magnification of the amplifies.

All samples had the first peak appearing at ~1.5 Å in R-space (Figure 13), which confirms that the distances of Zn-O in four batch experiments were similar. A double peak structure is shown at ~2-3 Å for BT1, BT2 and BT3 and at ~2.2-3.4 Å for BT4, suggests that there are two subshells in that R region.

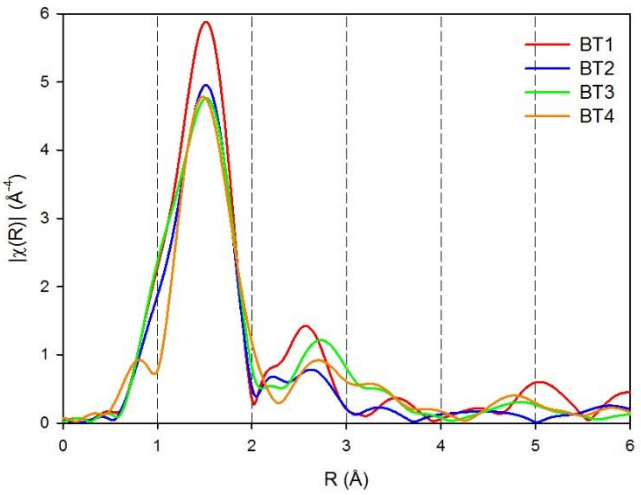

Figure 13 Experimental EXAFS spectra in R-space of all batch experiments.

The fitting results of the first shell of all four experiments suggest that the first shell is oxygen, and the Zn-O distance is 1.99 ± 0.01 Å and the coordination number is 3.8 ± 0.3. This Zn-O distance and coordination number is consistent with Waychunas et al. (2003), who reported a similar Zn-O distance of 1.97± 0.1 Å, and a coordination number of 4± 0.5, when Zn complexes on a surface of 2-line ferrihydrite samples. The local structure information of the first shell was also consistent with Juillot et al. (2011), who stated that when Zn is adsorbed onto 2-Line ferrihydrite, the Zn-O distance is1.96 Å and the coordination number is 3.2. A comparison was conducted between the samples from this study and previously reported Zn precipitates, based on the local structure information of the first shell (Table 9). The tetrahedral oxygen coordination observed in the solid samples differs from the octahedral oxygen coordination of $Zn(H_2O)_6^{2+}$ present in the initial solutions of all of the batch experiments, which has a Zn-O distance of 2.11± 0.2 Å, and a coordination number of 6 or 7.

Table 9 First shell comparison between reference materials and samples in this study

Compound	CN	(Å)	Mechanisms	References
N/A	3.8 ± 0.3	1.99 ± 0.01	N/A	This study
ZnO (zincite)	4	1.978	Precipitation	Kihara and Donnay (1985)

$ZnFe_2O_4$ (franklinite)	4	1.99	Co-precipitation	Hill et al. (1979)
γ-$Zn(OH)_2$	4	1.96	Precipitation	Christensen (1969)
ε-$Zn(OH)_2$ (Wülfingite)	4	1.96	Precipitation	Schnering (1964)
Zn adsorbed to 2-lines ferrihydrite	3.2	1.96	Adorption	Juillot et al. (2011)
Zn adsorbed to 2-lines ferrihydrite	4± 0.5	1.97± 0.1	Adorption	Waychunas et al. (2003)

Based on the specific reaction environment observed in this study (i.e. Zn (II) solution reacted with ZVI), there are five possible models for the Zn local structural environment of the second and third shell (Table 10). These five models include the possible Zn products associated with different removal mechanisms.

Table 10 Five models for Zn local structural environment

Model	First shell	Second shell	Third shell
1	Zn-O	Zn-Fe	Zn-Fe
2	Zn-O	Zn-O	Zn-Fe
3	Zn-O	Zn-Zn	Zn-Zn
4	Zn-O	Zn-O	Zn-Zn
5	Zn-O	Zn-Fe	Zn-Zn

R-space curve fitting of the experimental data from BT1, BT2, BT3 and BT4 was performed using these five models; during this comparison, attention focused on the magnitude of the Fourier Transform (FT) and the imaginary part of the FT. Considering the residual in terms of the whole R region, the second shell magnitude and imaginary parts of second shell, fitting results are summarized in Table 11.

Table 11 R space curve fitting result for four batch experiments

Experiment	Model	configuration	Shell	Path	CN	R	DW	Total Fitting Residual	E_0
BT1	1	Zn-O-Fe-Fe	1	Zn-O	3.9	1.99	0.0059[1]	11.3	-0.5
			2	Zn-Fe	0.8	2.70	0.0009[1]		
			3	Zn-Fe	0.7	3.01	0.0100[2]		
	2	Zn-O-O-Fe	1	Zn-O	3.8	1.98	0.0059[1]	15.4	-1.2
			2	Zn-O	1.8	2.66	0.0009[1]		
			3	Zn-Fe	1.0	3.06	0.0094		
	3	Zn-O-Zn-Zn	1	Zn-O	3.9	1.99	0.0059[1]	10.5	-0.4
			2	Zn-Zn	0.9	2.68	0.0009[1]		
			3	Zn-Zn	0.4	2.98	0.0100[2]		
	4	Zn-O-O-Zn	1	Zn-O	3.7	1.98	0.0059[1]	16.3	-1.2
			2	Zn-O	1.7	2.65	0.0009[1]		
			3	Zn-Zn	0.8	3.04	0.0072		
	5	Zn-O-Fe-Zn	1	Zn-O	3.9	1.99	0.0059	11.8	-0.7
			2	Zn-Fe	0.7	2.69	0.0059[1]		
			3	Zn-Zn	0.7	3.01	0.0100[2]		
BT2	1	Zn-O-Fe-Fe	1	Zn-O	3.7	1.98	0.0075	8.2	-1.9
			2	Zn-Fe	0.4	2.72	0.0075[1]		
			3	Zn-Fe	0.4	3.16	0.0095		
	2	Zn-O-O-Fe	1	Zn-O	3.6	1.98	0.0072	9.8	-2.2
			2	Zn-O	0.8	2.69	0.0072[1]		
			3	Zn-Fe	0.7	3.15	0.0100[2]		
	3	Zn-O-Zn-Zn	1	Zn-O	3.7	1.98	0.0075	8.0	-1.9
			2	Zn-Zn	0.6	2.71	0.0100[2]		
			3	Zn-Zn	0.5	3.17	0.0100		

	4	Zn-O-O-Zn	1	Zn-O	3.7	1.98	0.0075	23.3	-2.3
			2	Zn-O	0.9	2.69	0.0075[1]		
			3	Zn-Zn	0.6	3.13	0.0087		
	5	Zn-O-Fe-Zn	1	Zn-O	3.7	1.98	0.0075	8.5	-1.9
			2	Zn-Fe	0.4	2.72	0.0075[1]		
			3	Zn-Zn	0.5	3.15	0.0100[2]		
BT3	1	Zn-O-Fe-Fe	1	Zn-O	3.5	2.00	0.0075[1]	10.9	-0.5
			2	Zn-Fe	0.2	2.68	0.0075[1]		
			3	Zn-Fe	1.0	3.19	0.0075[1]		
	2	Zn-O-O-Fe	1	Zn-O	3.5	1.99	0.0075[1]	12.4	-0.6
			2	Zn-O	0.4	2.67	0.0075[1]		
			3	Zn-Fe	1.1	3.18	0.0075[1]		
	3	Zn-O-Zn-Zn	1	Zn-O	3.4	2.00	0.0075[1]	8.5	-0.3
			2	Zn-Zn	0.4	2.67	0.0075[1]		
			3	Zn-Zn	1.1	3.18	0.0075[1]		
	4	Zn-O-O-Zn	1	Zn-O	3.4	2.00	0.0075[1]	18.2	-0.2
			2	Zn-O	0.4	2.67	0.0075[1]		
			3	Zn-Zn	2.7	3.14	0.0075[1]		
	5	Zn-O-Fe-Zn	1	Zn-O	3.5	2.00	0.0075[1]	9.1	-0.5
			2	Zn-Fe	0.3	2.68	0.0075[1]		
			3	Zn-Zn	1.0	3.17	0.0075[1]		
BT4	1	Zn-O-Fe-Fe	1	Zn-O	3.9	1.99	0.0091	14.4	-2.5
			2	Zn-Fe	0.4	2.65	0.0091[1]		
			3	Zn-Fe	1.1	3.55	0.0100[2]		
	2	Zn-O-O-Fe	1	Zn-O	3.7	1.96	0.0084	13.6	-6
			2	Zn-O	1.4	2.56	0.0084[1]		
			3	Zn-Fe	1.3	3.51	0.0100[2]		

	3	Zn-O-Zn-Zn	1	Zn-O	4.0	1.98	0.0091	13.5	-3.5
			2	Zn-Zn	0.6	2.63	0.0100[2]		
			3	Zn-Zn	1.2	3.53	0.0100[2]		
	4	Zn-O-O-Zn	1	Zn-O	3.7	1.96	0.0084	13.8	-6
			2	Zn-O	1.3	2.56	0.0084[1]		
			3	Zn-Zn	1.4	3.5	0.0100[2]		
	5	Zn-O-Fe-Zn	1	Zn-O	4.1	1.98	0.0096	13.1	-3.8
			2	Zn-Fe	0.5	2.64	0.0100[2]		
			3	Zn-Zn	1.3	3.52	0.0100[2]		

1. Low limit; 2. High limit.

Based on an examination of the residuals (Figure 14), the experimental data of BT1 can be better fitted with model 1, model 2 and model 3; BT3 and BT4 can be better fitted with model 3 and model 5. The fitting residual of BT2 is lower compare to BT1, BT3, and BT4, and BT2 can be better fitted using model 1, model 2, and model 3. The lower residual of BT2 suggested that the reaction in BT2 might be different to the other three batch experiments. All four batch experiments can not be fit with model 2 or model 4 (Figure 14). The second shell cannot be oxygen. Unlike the initial solutions, in which two shells of water surround each Zn, no water molecules are present within the inner-sphere of Zn associated with the solid phase. Fitting for all four samples suggests a double metallic coordination at the second FT peak in the R region. However, both Zn-Zn and Zn-Fe can fit the second shell, with a small effect on the Zn-M (M=Zn, or Fe, or both) distance and coordination number.

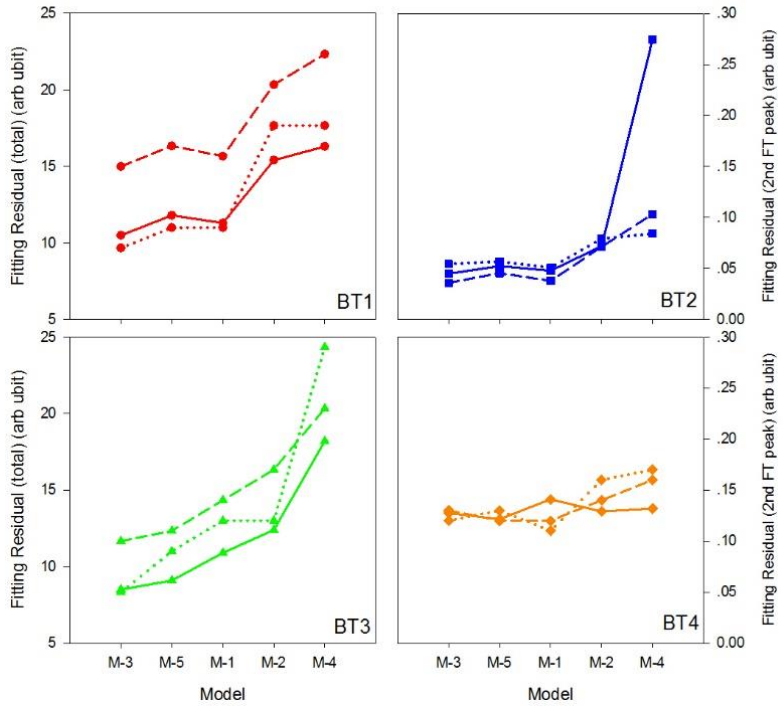

Figure 14 EXAFS fitting residual in terms of the whole R region (total magnitude with solid line), second shell FT magnitude (dot line) and second shell FT imaginary (dash line) of 5 testing models listing in Table 10. The lower the residual is, the better the testing model matches the experimental data.

A comparison between the R space curve-fitting results, based on the three shell models (a) Zn-O-Fe-Fe (Model 1 in Table 11), (b) Zn-O-Zn-Zn (Model 3 in Table 11) and (c) Zn-O-Fe-Zn (Model 5 in Table 11), respectively. The interatomic distance between center atom Zn and its second and third shell in different models in different batch experiments are listed in Table 12 and Table 13. The fitted interatomic distances among the three models for the corresponding scattering paths are very similar, indicating the limitation of the XAFS analysis, specifically for the system under investigation (i.e. Zn (II) solution reacted with ZVI).

The center atom Zn had tetrahedral geometry at distances between the center atom Zn and the second shell atom as summarized in Table 12. The distances in different test models and in samples from the batch experiments are similar, suggesting variations in Zn salt solutions and alkalinity concentrations assessed in these experiments did not influence the structure of the

second shell. Based on the EXAFS fitting, the possible model for second shell is ZnO_4-FeO_6 edge sharing on ferrihydrite. Without direct information on the structure of the alteration coating on Fe^0 the octahedron geometry of FeO_6 was based on goethite (Gualtieri and Venturelli, 1999). Tetrahedral geometry of ZnO_4 was based on R space curve fitting of the experimental data (Table 11, 12).

Table 12 Summary of the interatomic distance of second shell in R space curve fitting using model 1, 3 and 5

Model	Shell	Path	BT1	BT2	BT3	BT4
1	2	Zn-Fe	2.70	2.72	2.68	2.65
3	2	Zn-Zn	2.68	2.71	2.67	2.63
5	2	Zn-Fe	2.69	2.72	2.68	2.64
Average	2		2.69±0.01	2.71+0.01	2.67+0.01	2.64±0.01

The conceptual structure model of ZnO_4-FeO_6 (ferrihydrite type) edge sharing (Figure 15a) and Zn centered tetrahedron rotated vs O1-O2 axis (Figure 15b) reflect changes in the Zn-Fe bond length. Figure 16 shows how the Zn-Fe bond distance changes with the rotation angle. At a specific rotation angle, the Zn-Fe bond distance matches the fitted distance of the Zn-Fe bond. Thus, the ZnO_4-FeO_6 (ferrihydrite type) edge sharing model can explain the corresponding scattering paths in the second shell. In addition, this model can explain one of the Zn removal mechanisms, in which is Zn was removed by sorption onto ferrihydrite coating at the surface of ZVI.

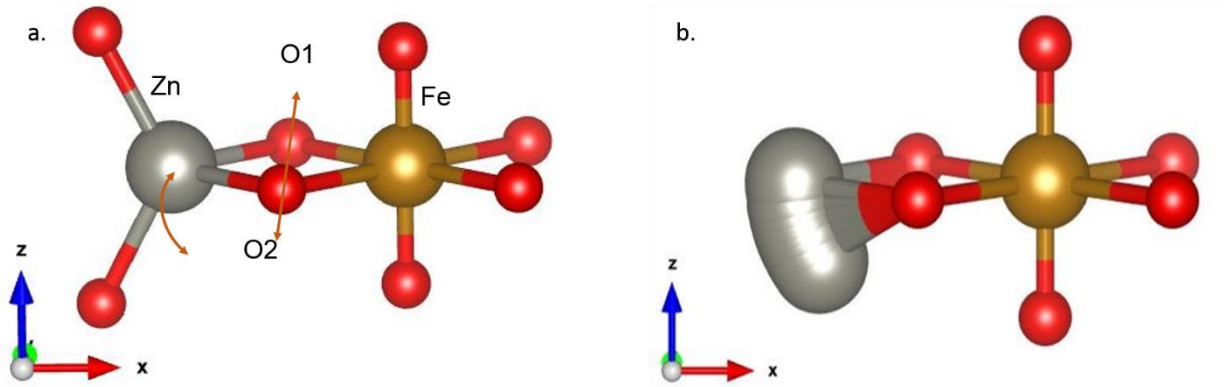

Figure 15 Conceptual structure model of ZnO_4-FeO_6 (ferrihydrite type) edge sharing mechanism for explaining the second shell EXAFS fitting results. The golden atom is Fe with octahedron geometry. The grey atom is Zn atom with tetrahedron geometry. The red atom is O, and Fe and Zn share O1 and O2. (a) is principle structure model, and (b) is the model when Zn centered tetrahedron is rotated vs O1-O2 axis.

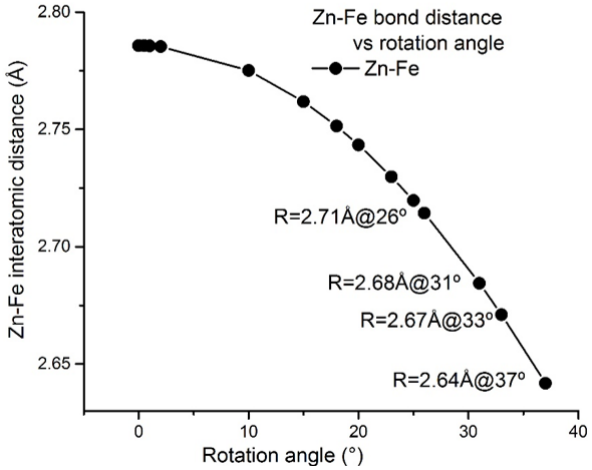

Figure 16. The ZnO_4-FeO_6 (ferrihydrite type) edge sharing conceptual model, showing changes in the Zn-Fe distance when the Zn centered tetrahedron is rotated.

The results for fitting the third shell and the distance between the center Zn atom and the third shell atom indicate that there is no significant difference in distance among models 1, 3 and 5 in the same batch experiment (Table 13). However, the distance in higher alkalinity batch experiments (BT3 and BT4) is longer compared to the same Zn salt in the ultra-pure water batch experiments (BT1 and BT2). In addition, compared to $ZnSO_4$, $ZnCl_2$ formed longer Zn-Zn/Fe bond distances in the third shell. Combining Zn removal mechanisms discussed in previous section to the structural information given by EXAFS fitting results, there are two possible

models in the third shell: (a) ZnO_4-ZnO_4 corner sharing of ZnO type and (b) ZnO_4-ZnO_4 corner sharing of $Zn(OH)_2$ type. Only one test model (i.e. ZnO_4-FeO_6 corner sharing of spinel type) was considered because Zn co-precipitated with Fe test model was analyzed, but the Zn-Fe distance was not within the range of EXAFS fitting results of the third shell.

Table 13 Summary of the interatomic distances of the third shell in R space curve fitting using models 1, 3 and 5

Model	Shell	Path	BT1	BT2	BT3	BT4
1	3	Zn-Fe	3.01	3.16	3.19	3.55
3	3	Zn-Zn	2.98	3.17	3.18	3.53
5	3	Zn-Zn	3.01	3.15	3.17	3.52
Average	3		3.00±0.02	3.16±0.01	3.18±0.01	3.53±0.02

In the first test model, the third shell includes ZnO_4-ZnO_4 corner sharing of the ZnO type, which is consistent with surface precipitated zinc oxide. This ZnO_4 structure is based on the structure of mineral zincite (Kihara and Donnay, 1985), and is consistent with the conceptual model shown in Figure 17. When the bond angle between Zn1-O and Zn2-O is changed systematically, the Zn1-Zn2 distance changes simultaneously. The correlation between the bond angle and the Zn1-Zn2 distance was determined by geometry calculations, and the relationship shown in Figure 18.

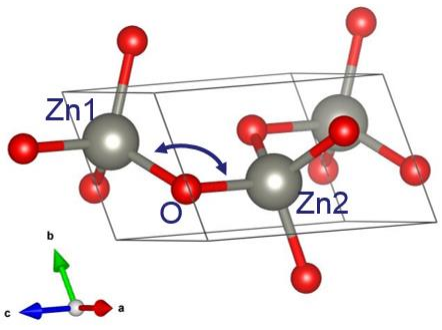

Figure 17 A conceptual model of ZnO surface precipitation/ The grey atom is Zn, and the red atom is O. Two ZnO_4 units share an O atom, and the bond angle can change within a limited range.

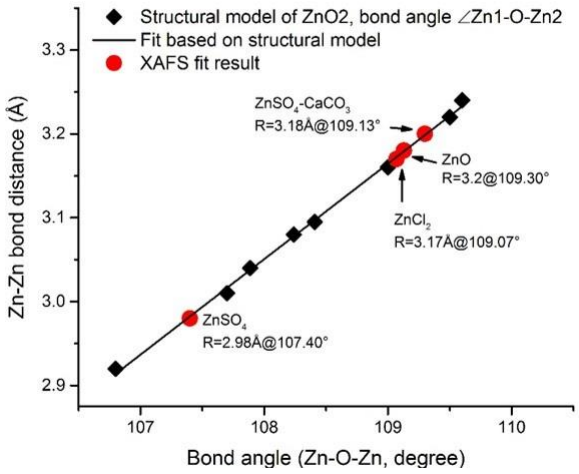

Figure 18. The relationship between bond angle Zn1-O-Zn2 and interatomic distance Zn-Zn in ZnO model.

The corner sharing ZnO type of ZnO_4 tetrahedron can address the Zn-Zn coordination distances observed for the for BT1, BT2 and BT3 experiments, with a Zn1-O-Zn2 bond angle 107.4º, 109.07º and 109.13º respectively. However, this configuration cannot accommodate the fitting results for BT4.

For BT4, shell models 3 and 5 point to a Zn-Zn distance of 3.52 to 3.53 Å, which is consistent with the average Zn-Zn distance of the third shell Zn-Zn coordination of γ-$Zn(OH)_2$ type at 3.53 Å. The ZnO_4-ZnO_4 corner sharing with a γ-$Zn(OH)_2$ type structure can explain the Zn speciation in the third shell of BT4 (Figure 19).

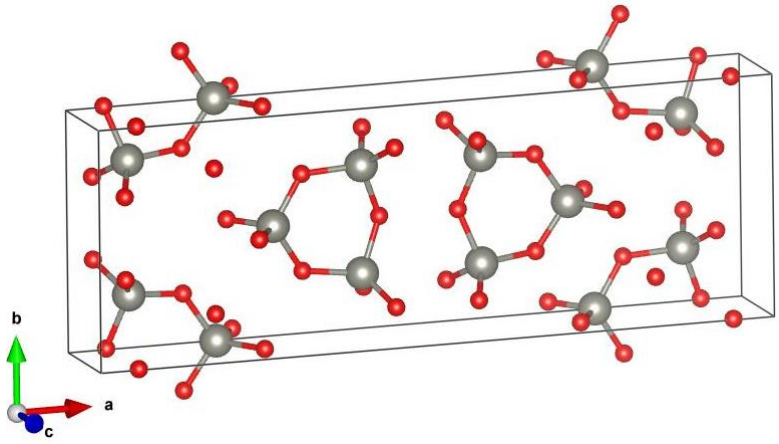

Figure 19 Conceptual model of ZnO_4-ZnO_4 corner sharing with γ-$Zn(OH)_2$. Grey atom is Zn, and red atom is O. Three Zn share three O.

All samples of four batch experiments have ZnO_4 tetrahedron geometry in the first shell with similar Zn-O bond distances. The Zn coordination geometry changed from octahedral (in the initial solution) to tetrahedral (solid phase). In the second shell, there is no significant difference among samples of different batch experiments. Zinc tetrahedral bonded with octahedral Fe hydroxide (Fe from ferrihydrite) sharing two oxygen atoms (edge sharing) provides the best match to the EXAFS results. These observations suggest that one of the Zn removal mechanisms is Zn absorption onto a ferrihydrite-type solid surface, which was produced by the reaction between ZVI and water. However, without the local structural information of this Fe hydroxide phase, no further information can be confirmed. Both the Zn-Zn path and the Zn-Fe path were tested for the third shell for comparison with EXAFS results. However, Zn-O-Fe-Fe test model failed to match the EXAFS fitting results. Thus, for the third shell, two types of ZnO_4-ZnO_4 corner sharing mechanisms, i.e., with ZnO and γ-$Zn(OH)_2$, are suggested by fitting the by XAFS results. This outcome suggests that, Zn precipitation forming ZnO and $Zn(OH)_2$, provides another Zn removal mechanism. The structure of $Zn(OH)_2$ may or may not have changed during the freeze-drying process, and the structure of $Zn(OH)_2$ might be similar to ZnO or keeping original $Zn(OH)_2$ structure. Thus, using only EXAFS fitting, $Zn(OH)_2$ and ZnO

production cannot be clearly discerned. In addition, from the EXAFS fitting results of the third shell, the experimental system with higher alkalinity has a longer Zn-Zn bond distance in the third shell. This observation suggests that alkalinity did change the structure produced during Zn precipitation, although it did not influence the coordination number.

2.4.5 Isotope Fractionation

Zinc removal in the duplicate experiments (A and B) followed similar trends (Figure 5), additionally the aqueous Zn species in the duplicates were in agreement when modeled using PHREEQC (Table 6 and Table 7). Isotope ratio measurements were only determined for one of the replicates (A) to evaluate the relationship between isotope fractionation and removal mechanisms in the different experiments.

In this study isotope $^{66/64}$Zn was measured on the unreacted Zn in the solution phase rather than digesting the solid phase. Balistrieri et al. (2008) and Juillot et al. (2008) suggest that measuring isotope fractionation in the solution is preferable as: 1) when solid phase is filtered to separate it from the solution, the solid phase may retain some of the unreacted solution on the surface. Therefore, if this solid phase is digested, the Zn isotope ratio will be a mixture of Zn on the solid phase and Zn in solution; 2) if the solid phase was washed before digestion, the pH environment would be changed. Zinc sorption is significantly influenced by pH and Zn may be desorbed during washing and; 3) Zn might either absorb to or co-precipitate onto the solid phase (ZVI) or be suspended in the solution retained on the filters. Hence, it is necessary to digest not only the solid phase but also the filters. Digestion of the solid phase and filters might pose a challenge during isotope purification. For example, these experiments contain ZVI, which may dissolve during the digestion, leading to the potential for the concentration of dissolved Fe (which is an isobaric interference on Zn isotope measurement) to exceed the concentration of Zn;

additionally, organic materials or other metals may be released to solution.

The notation for the isotopic ratios ($\delta^{66}Zn$) used in following discussion describes the isotopic fractionation occurring in the aqueous phase, rather than the solid phase. The isotopic composition of the stock input solution was normalized to daily measurements of IRMM-3702. Considering the uncertainty associated with the measurements there was no significant difference ($p > 0.05$) in the $\delta^{66}Zn$ of the different input solutions ($ZnCl_2$, $ZnSO_4$ or changes in alkalinity Table 14). These $\delta^{66}Zn$ values are similar to those reported by Veeramani et al., (2015), reported $\delta^{66}Zn$ of solutions using $ZnSO_4$ and $ZnCl_2$ salts were -0.21±0.04‰ and -0.14±0.03‰ respectively.

Table 14 Normalized $\delta^{66}Zn$ of input solutions of all four batch experiments.

BT1	BT2	BT3	BT4
-0.20±0.04‰	-0.18±0.09‰	-0.21±0.04‰	-0.17±0.08‰

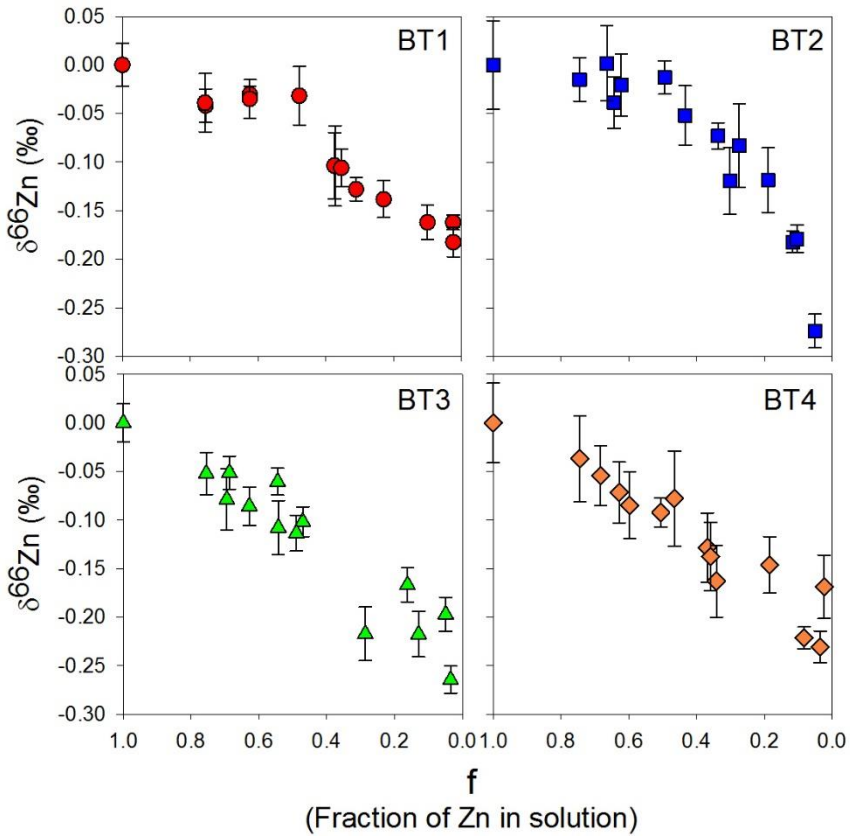

Figure 20 Normalized isotopic value ($\delta^{66}Zn$) of the solution as a function of fraction of Zn in solution in all four batch experiments. The error bars represent the 2σ uncertainty due to separations and MC-ICP-MS measurement.

In order to compare the isotope fractionation in the different batch experiments, the $\delta^{66}Zn$ values have been reported relative to the isotopic composition of the starting solution (Figure 20), hence each batch experiment plot starts with a zero $\delta^{66}Zn$.

Similar isotopic behavior was observed in all of the experiments, the $\delta^{66}Zn$ decreased relative to the composition of the starting solution as Zn was removed from solution (Figure 20). After 288 hours, 95% or more Zn was removed from solution, and the $\delta^{66}Zn$ in BT1, BT2, BT3 and BT4 declined from 0 ‰ to -0.18±0.03‰, -0.27±0.03‰, -0.26±0.03‰, -0.17±0.07‰, respectively.

The fractionation observed here is significant in comparison to analytical uncertainties

(0.07 ‰). The preferential removal of the heavier Zn isotope leads to an enrichment of the lighter isotope in solution. These results are in agreement with Balistrieri et al. (2008) and Juillot et al. (2008), who found an enrichment of the lighter Zn isotopes in the solution phase when Zn was adsorbed onto 2-Line ferrihydrite, goethite and amorphous Fe (III) oxyhydroxide. Pokrovsky et al. (2005) reported a negative fractionation in the supernatant during Zn sorption onto hematite, corundum and gibbsite; however, a positive Zn fractionation was also reported sorption of Zn onto goethite which is inconsistent with the observations of Balistrieri et al. (2008) and Juillot et al. (2008). In addition, during the precipitation of hydrozincite ($Zn_5(CO_3)_2(OH)_6$) the heavier Zn isotopes were preferentially removed from solution leaving the remaining solution enriched in the lighter isotopes (Veeramani et al., 2015).

The Zn concentration and $\delta^{66}Zn$ in the supernatant decreased throughout the experiments (from 0 hours to 288 hours), and the reaction did not reach equilibrium. Hence, the behavior of Zn concentration and $\delta^{66}Zn$ upon the whole removal process was kinetically limited. Mass-dependent fractionation was examined by plotting $\delta^{67}Zn$ and $\delta^{70}Zn$ of all of the samples as a function of $\delta^{66}Zn$ (Figure 21). The slopes of the $\delta^{67}Zn$ vs $\delta^{66}Zn$ and $\delta^{70}Zn$ vs $\delta^{66}Zn$ relationships were 1.4902 and 2.9163, respectively (Figure 21). The theoretically calculated results from the exponential law (kinetic expression) of the slopes of $\delta^{67}Zn$ vs $\delta^{66}Zn$ and $\delta^{70}Zn$ vs $\delta^{66}Zn$ were 1.490 and 2.915 (Matthies et al., 2014). The slopes determined by this research and the theoretically calculated slopes are comparable; thus, the results can be discussed in term of mass-dependent isotope fractionation.

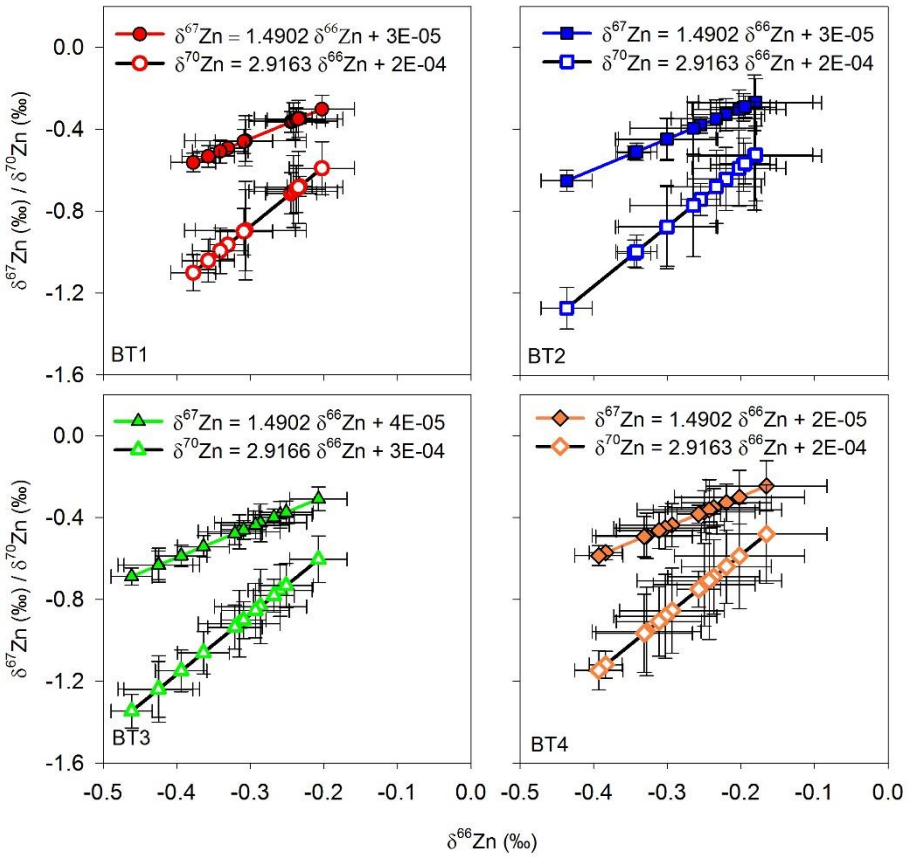

Figure 21 $\delta^{67}Zn$ and $\delta^{70}Zn$ as a function of $\delta^{66}Zn$ of all measured samples. The external reproducibility of the measurements is ±0.2‰ (2σ).

Zinc removal in this study is attributed to non-equilibrium (kinetic) processes, in which the back reaction between the reactant and product is negligible. Another Zn accumulation experiment was set up under similar experimental conditions (i.e. the same volume and concentration of Zn in the input solution, mass of ZVI, temperature and humidity, etc.) however the input solution was replaced every 5 days. Zinc was still removed from solution after 8 cycles. This observation suggests that, compared to the surface area of ZVI, there is a limited Zn supply in solution. Zinc isotopes in the solutions did not reach an isotopic equilibrium after 288 hours, as $\delta^{66}Zn$ kept decreasing through the entire experiment.

A reaction system can be considered an “irreversible” system or a “reversible” system. If

formation of the Zn reaction product is irreversible and will not react with the solution, the reaction product was isolated from the solution, and the system is “irreversible” system. On the contrary, in a “reversible” system, the removed Zn can still equilibrate with aqueous Zn. When Zn was removed from solution by irreversible precipitation, Veeramani et al. (2015) used a Rayleigh fractionation model to describe the Zn isotope fractionation as a function of the fraction of remaining fraction of aqueous Zn (*f*). Pokrovsky et al. (2005), Balistrieri et al. (2008) and Juillot et al. (2008) used an equlibrium model in a "reversible" system to describe the process when Zn is removed by adsorption.

To evaluate whether the reactions in this research were occurring in an "irreversible" system or a "reversible" system, both the Rayleigh fractionation and equilibrium models were applied to calculate the theoretical δ^{66}Zn remaining in the solution as a function of *f* in an “irreversible” system and in a “reversible” system to the measured ones. In theoretical plotting δ^{66}Zn as a function of f should either fit the Rayleigh model (“irreversible” system, Equation 17) or equilibrium model (“reversible” system, Equation 18).

(17) $$\delta^{66}Zn = \left[f^{(\alpha-1)} - 1 \right] \times 1000‰$$

(18) $$\delta^{66}Zn = \frac{(1-f)\times(\alpha-1)}{(1-f)+\alpha f} \times 1000‰$$

where *f* is the fraction of Zn in solution, and α is the fractionation factor. There is a α in Equation 17 and in Equation 18, which can be used to compare the isotope fractionation in the four batch experiments; however, the fractionation factor α will be calculated to different values in the same experiment but use different fitting models (Rayleigh model or equilibrium model). For this reason, the fractionation factor α can be used to compare different experiments only if they used the same fitting method. Equation 17 and Equation 18 were respectively used to fit four sets of measured “δ^{66}Zn vs. *f*" using SigmaPlot (v11.0) and the fractionation factor of each batch

experiment and uncertainty of each fitting was given at the same time (Figure 22).

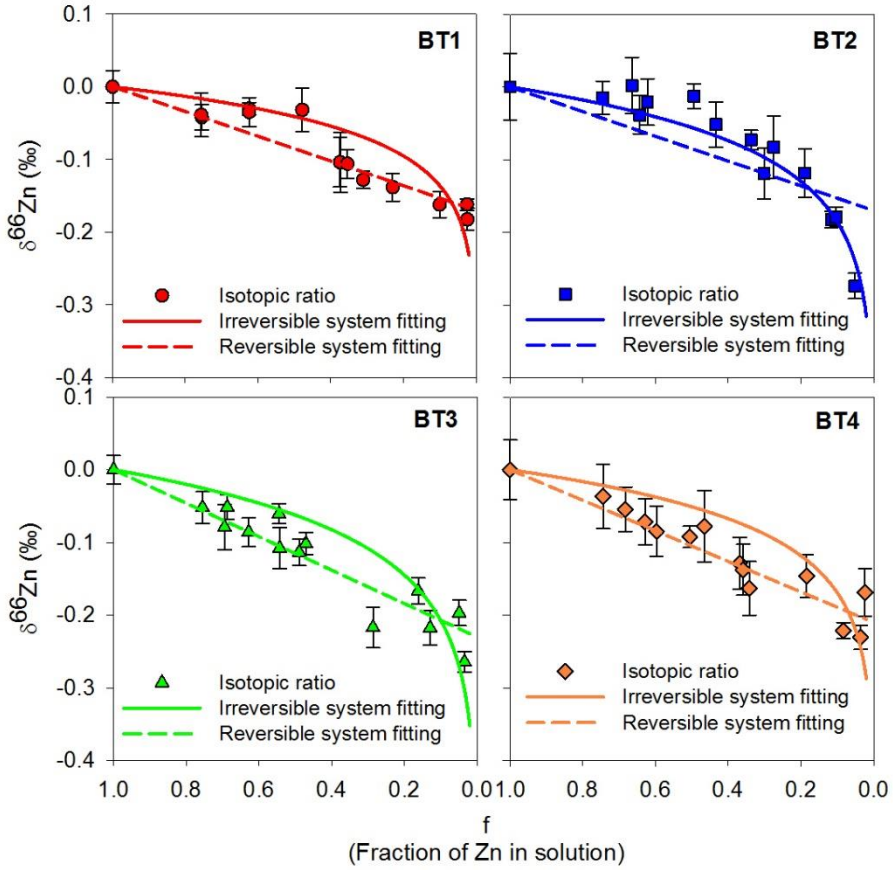

Figure 22 Evolution of isotopic ratios ($\delta^{66}Zn$) as a function of the fraction of Zn in solution for all batch experiments. Solid lines represent the theoretical calculation considered the system as an open system, and used Rayleigh Equation. Dashed lines were the theoretical calculation only considered the system as a closed system, and used equilibrium fitting. Error bars represents the external reproducibility.

The "irreversible" and "reversible" system fitting are compared in Figure 22. The calculated fractionation factors (α) and uncertainties (σ) are shown in Table 15. An R^2 statistic was used to assess the goodness of fit. The factors indicating an "irreversible" system are in grey shaded rows in Table 15, and the factors indicating a "reversible" system are in the white rows in Table 15.

Table 15 Comparison between irreversible system fitting and reversible system fitting

	BT1	BT2	BT3	BT4
α_{irre}	1.000059085	1.000080704	1.000090014	1.000073466

ε_{irre}	0.06±0.04	0.08±0.02	0.09±0.05	0.07±0.05
R^2 (irreversible)	0.5923	0.9268	0.6115	0.4231
α_{re}	0.99983	0.99983	0.99977	0.99979
Δ_{re}	-0.17±0.02	-0.17±0.05	-0.23±0.03	-0.21±0.02
R^2 (reversible)	0.8753	0.6394	0.8863	0.8988

The R^2 values were used to compare how different models fit the data from the four batch experiments. BT2 was a better fit with Rayleigh model, which has R^2= 0.9268, whereas BT1, BT3 and BT4 were a better fit with an equilibrium model (R^2= 0.8753, 0.8863 and 0.8988, respectively). This fitting results suggested an "irreversible" reaction process, such as adsorption, might be the removal mechanism in BT2, while a "reversible" reaction process, such as precipitation, might be the dominant removal mechanism in BT1, BT3, and BT4. In consideration of the discussion in previous sections, this difference might be due to the presence of oxygen in BT2, which resulted in lower pH values, remaining below pH 5 for the initial 4-24 hours of the experiment. These low pH values may have limited the extent of $Zn(OH)_2$ precipitation, and influenced the extent of Zn isotope fractionation. Furthermore, the accumulation of ferric oxyhydroxides may have provided a greater abundance of substrate for Zn adsorption in BT2. During the initial 100 hours of the experiment the δ^{66}Zn values in experiment BT2 fell above the equilibrium fractionation trend. In BT2, enrichment factor (ε) (definition in Equation 8), can be used to compare to other Zn isotope fractionation research in "irreversible" systems. In BT1, BT3, and BT4, separation factor (Δ) (definition in Equation 9) can be used to compare Zn isotope fractionation in "reversible" systems.

Compared to the enrichment factor ε in BT2 (0.08‰±0.02‰), Veeramani et al. (2015) reports a more positive value of ε during Zn precipitation forming hydrozincite (ε= 0.18‰). However, forming different Zn precipitation products would result in differences in isotope fractionation. Because there is no information on Zn isotope fractionation during formation of

ZnO and $Zn(OH)_2$ precipitation, Zn isotope fractionation in this study cannot discern if the Zn removal is by precipitation of ZnO and $Zn(OH)_2$.

Veeramani et al. (2015), did not observe fractionation of Zn in experiments in which Zn was adsorbed by ferrihydrite at pH= 7.2, because the Zn isotope ratios did not change as a function of time. Similar to their work, the initial concentration of Zn input solution was 0.08 M and $ZnCl_2$ was chosen as one of Zn input solutions. However, their work was conducted with a lower solid:liquid ratio (2 g L^{-1}) than this study (33.33 g L^{-1}). However, considering that the XAFS results suggest that Zn was removed by adsorption Zn to Fe (oxyhydroxides), which constituted a minor fraction of the total ZVI mass, the concentration of adsorbate (Fe hydroxides) was unknown.

Separation factors of BT1, BT3 and BT4, which represent Zn fractionation in solution ($\Delta_{solution\text{-}ZVI}$), were -0.17‰± 0.02‰, -0.23‰± 0.03‰, and -0.21‰± 0.02‰, respectively. The $\Delta_{solution\text{-}ZVI}$ values for BT1 were lower than BT3 and BT4; however, according to the t-test ($p>0.05$), there is no significant difference between these enrichment factors. Previous research on Zn isotope fractionation during Zn adsorption onto iron oxides or hydroxides is summarized in Table 16.

Table 16 Summary of the previous research on Zn isotope fractionation during Zn adsorption onto iron oxides or hydroxides solid phases

Adsorbate	Separation factor ($\Delta_{solution\text{-}solid}$) (‰)	Citation
Hematite	-0.2±0.5	Pokrovsky et al. (2005)
Goethite	0.2±0.03	Pokrovsky et al. (2005)
	-0.15±0.08	Cacaly et al. (2004)
	-0.29	Juillot et al. (2008)
Amorphous Fe(III)	-0.58±0.08	Cacaly et al. (2004)

oxyhydroxide	-0.52±0.04	Balistrieri et al. (2008)
2-lines ferrihydrite	-0.53	Juillot et al. (2008)
	N/A	Veeramani et al. (2015)
Corrosion of ZVI in ultra-pure water/ $CaCO_3$ solution	-0.17±0.02	This study BT1
	-0.17±0.05	This study BT2
	-0.23±0.03	This study BT3
	-0.21±0.02	This study BT4

Negative fractionation of $\delta^{66}Zn$ was observed in all the previous studies except for Zn sorption on to hematite (Pokrovsky et al., 2005). Thus the heavier isotope of Zn (i.e. ^{66}Zn) preferentially adsorbed onto the solid phase and leaving the lighter isotope (i.e. ^{64}Zn) in solution resulting in a negative fraction (Balistrieri et al. 2008; Pokrovsky, et al. 2005). Compared to these previous studies, the extent of Zn isotope fractionation in this study is most similar to the experiments which used hematite and goethite as adsorbates, whereas experiments with amorphous Fe(III) oxyhydroxide and 2-line ferrihydrite showed greater Zn isotope fractionation. Thus, Zn isotope fractionation depends on the structure of the adsorbate.

Chapter 3: Conclusion and environmental implications

3.1 Summary of Findings

Four batch experiments were conducted to characterize the Zn isotope fractionation during reaction of $Zn^{2+}_{(aq)}$ with ZVI and to compare how different Zn solutions ($ZnSO_4$ vs. $ZnCl_2$) and alkalinity concentrations (ultra-pure water vs. 6 mg L^{-1} (as $CaCO_3$)) affected Zn and removal mechanisms and isotope fractionation. Decreases in Zn concentrations were associated with a decreasing $\delta^{66}Zn$ throughout the experiments. There is no significant different reaction rate among these four batch experiments. However, among these four batch experiments, samples of BT2, which used ultra-pure water and ZnCl2, reacted with the oxygen which is occasionally trapped in the glovebox. The consequences included low pH, and the difference in isotope fractionation and EXAFS modelling.

The concentration and $\delta^{66}Zn$ data of BT1, BT3 and BT4 can fitted equilibrium curve with different fractionation factors indicating that Zn(II) was not effectively isolated from the solution. The concentration and $\delta^{66}Zn$ data of BT2 can best be fit by a Rayleigh fractionation curve. Thus, fractionation factors of BT1, BT3, and BT4 derived from equilibrium fitting were compared to previous research that also used equilibrium fitting. Fractionation factors derived from these three batch experiments were similar, suggesting different Zn solutions or alkalinity concentrations did not significantly affect the extent of isotope fractionation. According to the results of XANES and EXAFS studies, the coordination number of Zn changed from six in initial solution to four in the first shell of Zn on solid ZVI. The bond between Zn and solid phase was stronger than Zn in solution, the heavier isotope ^{66}Zn was retained on the solid phase. Based on the possible EXAFS models for second shell and third shell of Zn, both adsorption and

precipitation are important removal mechanisms. Comparisons to previous studies indicate consistently negative fractionation factors, however, the degree of fractionation is dependent on the structure on the adsorbent solid.

3.2 Recommendation for future research

As dissolved Zn has one oxidation state, Zn was not reduced during the treatment by ZVI. Different Zn solutions and alkalinity did not have a significant effect on removal rate, attenuation efficiency, isotope fractionation, or removal mechanisms, suggesting that Zn isotope measurements can be widely used in different situations. Although Zn isotope measurements can provide an effective tool to track the extent of Zn attenuation during Zn transport, the use Zn isotope measurements in isolation are not sufficient to distinguish sorption-dominated and precipitation-dominated removal mechanisms. There is limited research reported $\delta^{66}Zn$ fractionation during Zn precipitation, especially $Zn(OH)_2$ and ZnO, this limited information constrains the application of Zn isotope measurements to determine reaction mechanisms in environmental systems.

.

References

Agrawal, Abinash, and Paul G. Tratnyek. 1996. "Reduction of Nitro Aromatic Compounds by Zero-Valent Iron Metal." *Environmental Science and Technology* 30(1): 153–60.

Balistrieri, Laurie S., David M. Borrok, Richard B. Wanty, and W. Ian Ridley. 2008. "Fractionation of Cu and Zn Isotopes during Adsorption onto Amorphous Fe(III) Oxyhydroxide: Experimental Mixing of Acid Rock Drainage and Ambient River Water." *Geochimica et Cosmochimica Acta* 72(2): 311–28.

Bigalke, Moritz, Stefan Weyer, Jozef Kobza, and Wolfgang Wilcke. 2010. "Stable Cu and Zn Isotope Ratios as Tracers of Sources and Transport of Cu and Zn in Contaminated Soil." *Geochimica et Cosmochimica Acta* 74(23): 6801–13. http://dx.doi.org/10.1016/j.gca.2010.08.044.

Blowes, D. W., Ptacek, C. J., Benner, S. G., McRae, C. W., Bennett, T. A., & Puls, R. W. (2000). Treatment of inorganic contaminants using permeable reactive barriers. *Journal of Contaminant Hydrology*, 45(1), 123-137. http://linkinghub.elsevier.com/retrieve/pii/S0169772200001224%5Cnhttp://linkinghub.elsevier.com/retrieve/pii/S0043135498003157%5Cnhttp://linkinghub.elsevier.com/retrieve/pii/S0043135499003887%5Cnhttp://www.tandfonline.com/doi/abs/10.1080/19443994.2013.778795%5Cnh.

Borrok, David M., David A. Nimick, Richard B. Wanty, and W. Ian Ridley. 2008. "Isotopic Variations of Dissolved Copper and Zinc in Stream Waters Affected by Historical Mining." *Geochimica et Cosmochimica Acta* 72(2): 329–44.

Bradl, Heike B. 2004. "Adsorption of Heavy Metal Ions on Soils and Soils Constituents." *Journal of Colloid and Interface Science* 277(1): 1–18.

Brooks, Clyde S. 1986. “Metal Recovery from Industrial Wastes.” *Journal of Metal* (July): 50–57.

Brown ID, and Poeppelmeier KR. Bond valences. Berlin (Heidelberg): Springer; 2014.

Bryan, Allison L., Shuofei Dong, Elise B. Wilkes, and Laura E. Wasylenki. 2015. “Zinc Isotope Fractionation during Adsorption onto Mn Oxyhydroxide at Low and High Ionic Strength.” *Geochimica et Cosmochimica Acta* 157: 182–97. http://dx.doi.org/10.1016/j.gca.2015.01.026.

Cantrell, Kirk J., Daniel I. Kaplan, and Thomas W. Wietsma. 1995. “Zero-Valent Iron for the in Situ Remediation of Selected Metals in Groundwater.” *Journal of Hazardous Materials* 42(2): 201–12.

Cloquet, Christophe, Jean Carignan, Moritz F. Lehmann, and Frank Vanhaecke. 2008. “Variation in the Isotopic Composition of Zinc in the Natural Environment and the Use of Zinc Isotopes in Biogeosciences: A Review.” *Analytical and Bioanalytical Chemistry* 390(2): 451–63.

Coplen, Tyler B. 2011. “Guidelines and Recommended Terms for Expression of Stable-Isotope-Ratio and Gas-Ratio Measurement Results.” *Rapid Communications in Mass Spectrometry : RCM* 25(17): 2538–60.

Deliyanni, E. A., E. N. Peleka, and K. A. Matis. 2007. “Removal of Zinc Ion from Water by Sorption onto Iron-Based Nanoadsorbent.” *Journal of Hazardous Materials* 141(1): 176–84.

Eisler, Ronald. 1988. “Contaminant Hazard Reviews Arsenic Hazards to Fish , Wildlife , and Invertabrates : A Synoptic Review.” *US Fish and Wildlife Service Contaminant Hazard Reviews* 85(12): 1–65. http://catalogue.nla.gov.au/Record/4005011.

Fernandez, Alvaro, and David M. Borrok. 2009. “Fractionation of Cu, Fe, and Zn Isotopes

during the Oxidative Weathering of Sulfide-Rich Rocks." *Chemical Geology* 264(1–4): 1–12. http://dx.doi.org/10.1016/j.chemgeo.2009.01.024.

Gélabert, A., Pokrovsky, O. S., Viers, J., Schott, J., Boudou, A., & Feurtet-Mazel, A. 2006. Interaction between zinc and freshwater and marine diatom species: surface complexation and Zn isotope fractionation. *Geochimica et Cosmochimica Acta* 70(4), 839-857.

Ha, Juyoung, François Farges, and GE Brown Jr. 2007. "Adsorption and Precipitation of Aqueous Zn (II) on Hematite Nano-and Microparticles." *X-Ray Absorption Fine Structure--XAFS* (November): 5–7. http://scholar.google.com/scholar?hl=en&btnG=Search&q=intitle:Adsorption+and+Precipitation+of+Aqueous+Zn+(+II+)+on+Hematite+Nano-+and+Microparticles#0.

Health Canada. 2012. "Guidelines for Canadian Drinking Water Quality Summary Table Prepared by the Federal-Provincial-Territorial Committee on Drinking Water of the Federal-Provincial-Territorial Committee on Health and the Environment March 2006." *Environments* (October 2014): 1–16.

Jamieson-Hanes, Julia H. et al. 2012. "Chromium Isotope Fractionation during Reduction of Cr(VI) under Saturated Flow Conditions." *Environmental Science and Technology* 46(12): 6783–89.

Jamieson-Hanes, J. H., Lentz, A. M., Amos, R. T., Ptacek, C. J., & Blowes, D. W. 2014. Examination of Cr (VI) treatment by zero-valent iron using in situ, real-time X-ray absorption spectroscopy and Cr isotope measurements. *Geochimica et Cosmochimica Acta* 142, 299-313.

Juillot, F., Maréchal, C., Ponthieu, M., Cacaly, S., Morin, G., Benedetti, M., & Guyot, F. 2008. Zn isotopic fractionation caused by sorption on goethite and 2-Lines ferrihydrite.

Geochimica et Cosmochimica Acta 72(19), 4886-4900.

Juillot, Farid et al. 2011. "Contrasting Isotopic Signatures between Anthropogenic and Geogenic Zn and Evidence for Post-Depositional Fractionation Processes in Smelter-Impacted Soils from Northern France." *Geochimica et Cosmochimica Acta* 75(9): 2295–2308.

Kafantaris, Fotios Christos A, and David M. Borrok. 2014. "Zinc Isotope Fractionation during Surface Adsorption and Intracellular Incorporation by Bacteria." *Chemical Geology* 366: 42–51. http://dx.doi.org/10.1016/j.chemgeo.2013.12.007.

Karabulut, Solmaz, Adil Denizli, and Yuda Yu. 2000. "Batch Removal of Copper (II) and Zinc (II) from Aqueous Solutions with Low-Rank Turkish Coals." *Separation and Purification Technology* 18: 177–84.

Katsoyiannis, Ioannis A., Andreas Voegelin, Anastasios I. Zouboulis, and Stephan J. Hug. 2015. "Enhanced As(III) Oxidation and Removal by Combined Use of Zero Valent Iron and Hydrogen Peroxide in Aerated Waters at Neutral pH Values." *Journal of Hazardous Materials* 297: 1–7. http://dx.doi.org/10.1016/j.jhazmat.2015.04.038.

Kavner, A., S. G. John, S. Sass, and E. A. Boyle. 2008. "Redox-Driven Stable Isotope Fractionation in Transition Metals: Application to Zn Electroplating." *Geochimica et Cosmochimica Acta* 72(7): 1731–41.

Klimkova, Stepanka et al. 2011. "Zero-Valent Iron Nanoparticles in Treatment of Acid Mine Water from in Situ Uranium Leaching." *Chemosphere* 82(8): 1178–84. http://dx.doi.org/10.1016/j.chemosphere.2010.11.075.

Kuzmin, a, S Obst, and J Purans. 1999. "X-Ray Absorption Spectroscopy and Molecular Dynamics Studies of Hydration in Aqueous Solutions." *Journal of Physics: Condensed Matter* 9(46): 10065–78.

Lemarchand, Emmanuel, Jacques Schott, and Jérôme Gaillardet. 2007. "How Surface Complexes Impact Boron Isotope Fractionation: Evidence from Fe and Mn Oxides Sorption Experiments." *Earth and Planetary Science Letters* 260(1–2): 277–96.

Li, Xiao-qin, and Wei-xian Zhang. 2007. "Sequestration of Metal Cations with Zerovalent Iron NanoparticlesA Study with High Resolution X-Ray Photoelectron Spectroscopy (HR-XPS)." *Journal of Physical Chemistry C* 111(19): 6939–6946. http://dx.doi.org/10.1021/jp0702189.

Lin, S. H., & Juang, R. S. 2002. "Heavy Metal Removal from Water by Sorption Using Surfactant-Modified Montmorillonite." *Journal of Hazardous Materials* 92(3): 315–26.

Lindberg, R. D., & Runnells, D. D. 1984. "Ground Water Redox Reactions: An Analysis of Equilibrium State Applied to Eh Measurements and Geochemical Modeling." *Science* 225(11): 925–27. http://go.galegroup.com.libproxy.wlu.ca/ps/i.do?id=GALE%7CA3406569&v=2.1&u=wate18005&it=r&p=AONE&sw=w&asid=66eab3f4e4f5124d026f5ca6cf8975bb.

Lindsay, Matthew B J, Carol J. Ptacek, David W. Blowes, and W. Douglas Gould. 2008. "Zero-Valent Iron and Organic Carbon Mixtures for Remediation of Acid Mine Drainage: Batch Experiments." *Applied Geochemistry* 23(8): 2214–25.

Maréchal, Chloé, and Francis Albarède. 2002. "Ion-Exchange Fractionation of Copper and Zinc Isotopes." *Geochimica et Cosmochimica Acta* 66(9): 1499–1509.

Maréchal, Chloé Nadia, Philippe Télouk, and Francis Albarède. 1999. "Precise Analysis of Copper and Zinc Isotopic Compositions by Plasma-Source Mass Spectrometry." *Chemical Geology* 156(1–4): 251–73.

Mason, Thomas F D et al. 2005. "Zn and Cu Isotopic Variability in the Alexandrinka Volcanic-Hosted Massive Sulphide (VHMS) Ore Deposit, Urals, Russia." *Chemical Geology* 221(3–

4): 170–87.

Matthies, R., L. Krahé, and D. W. Blowes. 2014. “Zinc Stable Isotope Fractionation upon Accelerated Oxidative Weathering of Sulfidic Mine Waste.” *Science of the Total Environment* 487(1): 97–101. http://dx.doi.org/10.1016/j.scitotenv.2014.04.020.

Matthies, Romy, Sean A. Sinclair, and David W. Blowes. 2014. “The Zinc Stable Isotope Signature of Waste Rock Drainage in the Canadian Permafrost Region.” *Applied Geochemistry* 48: 53–57. http://dx.doi.org/10.1016/j.apgeochem.2014.06.026.

Moeller, K., Schoenberg, R., Pedersen, R. B., Weiss, D., & Dong, S. 2012. Calibration of the New Certified Reference Materials ERM‐AE633 and ERM‐AE647 for Copper and IRMM‐3702 for Zinc Isotope Amount Ratio Determinations. *Geostandards and Geoanalytical Research* 36(2), 177-199.

Mokili, B, Y Charreire, R Cortes, and D Lincot. 1996. “Extended X-Ray Absorption Fine Structure Studies of Zinc Hydroxo-Sulphide Thin Films Chemically Deposited from Aqueous Solution.” *ELSEVI ER Thin Solid Films* 288: 21–28.

Nordstrom, D.K., F.D. Wilde. 2005. “Reduction-Oxidation Potential (Electrode Method).” *National Field Manual for the Collection of Water-Quality Data* 2: 1–22. papers2://publication/uuid/0FDC2EC6-A80F-4203-ABBF-EA965B51F0BE%5Cnpapers2://publication/uuid/176A0E24-2B83-488B-969D-D88B9936FE9B.

Nuttall, Charlotte A., and Paul L. Younger. 2000. “Zinc Removal from Hard, Circum-Neutral Mine Waters Using a Novel Closed- Bed Limestone Reactor.” *Water Research* 34(4): 1262–68.

Parkhurst, David L., and C.A.J. Appelo. 2013. “Description of Input and Examples for

PHREEQC Version 3 A Computer Program for Speciation , Batch-Reaction , One-Dimensional Transport , and Inverse Geochemical Calculations. U.S. Geological Survey Techniques and Methods, Book 6, Chapter A43, 497 P.

Plum, Laura M., Lothar Rink, and Haase Hajo. 2010. "The Essential Toxin: Impact of Zinc on Human Health." *International Journal of Environmental Research and Public Health* 7(4): 1342–65.

Pokrovsky, O. S., G. S. Pokrovski, J. Schott, and A. Galy. 2006. "Experimental Study of Germanium Adsorption on Goethite and Germanium Coprecipitation with Iron Hydroxide: X-Ray Absorption Fine Structure and Macroscopic Characterization." *Geochimica et Cosmochimica Acta* 70(13): 3325–41.

Pokrovsky, O. S., J. Viers, and R. Freydier. 2005. "Zinc Stable Isotope Fractionation during Its Adsorption on Oxides and Hydroxides." *Journal of Colloid and Interface Science* 291(1): 192–200.

Pokrovsky, Oleg S. et al. 2005. "Speciation of Zn Associated with Diatoms Using X-Ray Absorption Spectroscopy." *Environmental Science and Technology* 39(12): 4490–98.

Ravel, B., and M. Newville. 2005. "ATHENA, ARTEMIS, HEPHAESTUS: Data Analysis for X-Ray Absorption Spectroscopy Using IFEFFIT." *Journal of Synchrotron Radiation* 12(4): 537–41.

Reynolds, B. 2012. "Handbook of Environmental Isotope Geochemistry." (ii). http://link.springer.com/10.1007/978-3-642-10637-8.

Roberts, Darryl R., Robert G. Ford, and Donald L. Sparks. 2003. "Kinetics and Mechanisms of Zn Complexation on Metal Oxides Using EXAFS Spectroscopy." *Journal of Colloid and Interface Science* 263(2): 364–76.

Rodushkin, I., Stenberg, A., Andrén, H., Malinovsky, D., & Baxter, D. C. 2004. Isotopic fractionation during diffusion of transition metal ions in solution. *Analytical Chemistry*, 76(7), 2148-2151.

Rosman, KJR. Taylor, PDP. 1998. "Isotopic Compositions of the Elements 1997 (Technical Report)." *Pure and Applied Chemistry* 70(1): 217–35.

Rudge, John F., Ben C. Reynolds, and Bernard Bourdon. 2009. "The Double Spike Toolbox." *Chemical Geology* 265(3–4): 420–31. http://dx.doi.org/10.1016/j.chemgeo.2009.05.010.

Sheta, A. S. et al. 2003. "Sorption Characteristics of Zinc and Iron by Natural Zeolite and Bentonite." *Microporous and Mesoporous Materials* 61(1–3): 127–36.

Shrimpton, Heather K., David W. Blowes, and Carol J. Ptacek. 2015. "Fractionation of Selenium during Selenate Reduction by Granular Zerovalent Iron." *Environmental Science and Technology* 49(19): 11688–96.

Swedlund, Peter J., Jenny G. Webster, and Gordon M. Miskelly. 2009. "Goethite Adsorption of Cu(II), Pb(II), Cd(II), and Zn(II) in the Presence of Sulfate: Properties of the Ternary Complex." *Geochimica et Cosmochimica Acta* 73(6): 1548–62. http://dx.doi.org/10.1016/j.gca.2008.12.007.

Veeken, Adrie H M, Lawrence Akoto, Look W. Hulshoff Pol, and Jan Weijma. 2003. "Control of the Sulfide (S2-) Concentration for Optimal Zinc Removal by Sulfide Precipitation in a Continuously Stirred Tank Reactor." *Water Research* 37(15): 3709–17.

Veeramani, Harish et al. 2015. "Zinc Isotope Fractionation as an Indicator of Geochemical Attenuation Processes." *Environmental Science & Technology Letters*: acs.estlett.5b00273. http://pubs.acs.org/doi/10.1021/acs.estlett.5b00273.

Viers, Jérôme et al. 2007. "Evidence of Zn Isotopic Fractionation in a Soil-Plant System of a

Pristine Tropical Watershed (Nsimi, Cameroon)." *Chemical Geology* 239(1–2): 124–37.

Waychunas, G. A., C. C. Fuller, J. A. Davis, and J. J. Rehr. 2003. "Surface Complexation and Precipitate Geometry for Aqueous Zn(II) Sorption on Ferrihydrite: II. XANES Analysis and Simulation." *Geochimica et Cosmochimica Acta* 67(5): 1031–43.

Weiss, D. J. et al. 2005. "Isotopic Discrimination of Zinc in Higher Plants." *New Phytologist* 165(3): 703–10.

Wilkin, Richard T., and Mary S. McNeil. 2003. "Laboratory Evaluation of Zero-Valent Iron to Treat Water Impacted by Acid Mine Drainage." *Chemosphere* 53(7): 715–25.

Wilkinson, J. J., D. J. Weiss, T. F. D. Mason, and B. J. Coles. 2005. "Zinc Isotope Variation in Hydrothermal Systems: Preliminary Evidence From Theirish Midlands Ore Field." *Economic Geology* 100(3): 583–90.

Yamakawa, Akane, Katsuyuki Yamashita, Akio Makishima, and Eizo Nakamura. 2009. "Chemical Separation and Mass Spectrometry of Cr, Fe, Ni, Zn, and Cu in Terrestrial and Extraterrestrial Materials Using Thermal Ionization Mass Spectrometry." *Analytical Chemistry* 81(23): 9787–94.